DETECTION OF GAS HYDRATES IN GARDEN BANKS AND KEATHLEY CANYON FROM SEISMIC DATA

A Thesis

by

IDRIS MURAD

Submitted to the Office of Graduate Studies of
Texas A&M University
in partial fulfillment of the requirements for the degree of

MASTER OF SCIENCE

May 2009

Major Subject: Geophysics

DETECTION OF GAS HYDRATES IN GARDEN BANKS AND KEATHLEY CANYON FROM SEISMIC DATA

A Thesis

by

IDRIS MURAD

Submitted to the Office of Graduate Studies of
Texas A&M University
in partial fulfillment of the requirements for the degree of

MASTER OF SCIENCE

Approved by:

Chair of Committee,	John R. Hopper
Committee Members,	William W. Sager
	Richard L. Gibson
Head of Department,	Andreas K. Konenberg

May 2009

Major Subject: Geophysics

ABSTRACT

Detection of Gas Hydrates in Garden Banks and Keathley Canyon from Seismic Data.

(May 2009)

Idris Murad, B.S., Damascus University

Chair of Advisory Committee: Dr. John R. Hopper

Gas hydrate is a potential energy source that has recently been the subject of much academic and industrial research. The search for deep-water gas hydrate involves many challenges that are especially apparent in the northwestern Gulf of Mexico, where the sub-seafloor is a complex structure of shallow salt diapirs and sheets underlying heavily deformed shallow sediments and surrounding diverse minibasins.

Here, we consider the effect these structural factors have on gas hydrate occurrence in Garden Banks and Keathley Canyon blocks of the Gulf of Mexico. This was accomplished by first mapping the salt and shallow deformation structures throughout the region using a 2D grid of seismic reflection data. In addition, major deep-rooted faults and shallow-rooted faults were mapped throughout the area. A shallow sediment deformation map was generated that defined areas of significant faulting.

We then quantified the thermal impact of shallow salt to better estimate the gas hydrate stability zone (GHSZ) thickness. The predicted base of the GHSZ was compared to the seismic data, which showed evidence for bottom simulating reflectors and gas

chimneys. These BSRs and gas chimneys were used to ground-truth the calculated depth of the base of GHSZ.

Finally, the calculated GHSZ thickness was used to estimate the volume of the gas hydrate reservoir in the area after determining the most reasonable gas hydrate concentrations in sediments within the GHSZ. An estimate of 5.5 trillion cubic meters of pure hydrate methane in Garden Banks and Keathley Canyon was obtained.

ACKNOWLEDGEMENTS

I would like to thank my committee chair, Dr. John R. Hopper for his supervision and contribution to this research. I would like also to thank my committee member, Dr. William W. Sager for his guidance and comments and Dr. Richard L. Gibson, Jr. for his support throughout the course of this research.

Thanks also go to my colleagues Veronica Arrigoni, Luis Navarro, Dina Khalifa, Quefang Dou and Leslie Nemazi, and the department faculty and staff for their support. I also want to extend my gratitude to TGS-NOPEC geophysical company for providing the seismic data through Dr. William W. Sager.

TABLE OF CONTENTS

Page

LIST OF FIGURES

FIGURE Page

FIGURE Page

1. INTRODUCTION

Gas hydrate is an ice-like substance generated by the entrapment of gas molecules in a cage of water molecules (Sloan, 1998) (Figure 1). Gas hydrates occur naturally in shallow sediments in many deep-water environments and in permafrost regions at high latitudes where temperature and pressure conditions are suitable for both their formation and preservation. Because they may contain significant hydrocarbon accumulations, they have been proposed as an alternative energy source that could be exploited as conventional resources become depleted (Kvenvolden and McMenamin, 1980; Milkov and Sassen, 2001). In addition, gas hydrates are a potential hazard to oil drilling and production projects (Lerche and Noeth, 2002; Cooper and Hart, 2003).

The stability of gas hydrate is highly sensitive to a number of factors, including temperature, pressure, and chemistry, in particular salinity. The gas hydrate stability zone (GHSZ) is defined by where the temperatures are below the gas to solid phase transition. Figure 2 shows the basic principle. The bottom water temperature must be sufficiently low to be below the phase transition, otherwise hydrates will not form. The depth to the base of the stability zone is then determined by where the temperature curve in the sediments intersects phase curve (Kvenvolden and McMenamin, 1980; Sloan, 1998; Lerche and Noeth, 2002). While the basic concept is straightforward, both the

---

This thesis follows the style of Geophysics.

Figure 1. Chunks of a sub-seafloor gas hydrate sample. This sample was recovered from the northern Gulf of Mexico. The Schematic view on the center left is a gas hydrate crystal, which is composed of a cage of water molecules trapping a methane molecule. Gas hydrate is a combustible substance making it a potential source of energy (upper left) (after Winters and Lorenson, 2002).

geothermal gradient and phase curve are affected by the presence or absence of salt. Thus, detection of gas hydrates in areas in the Gulf of Mexico has proven challenging.

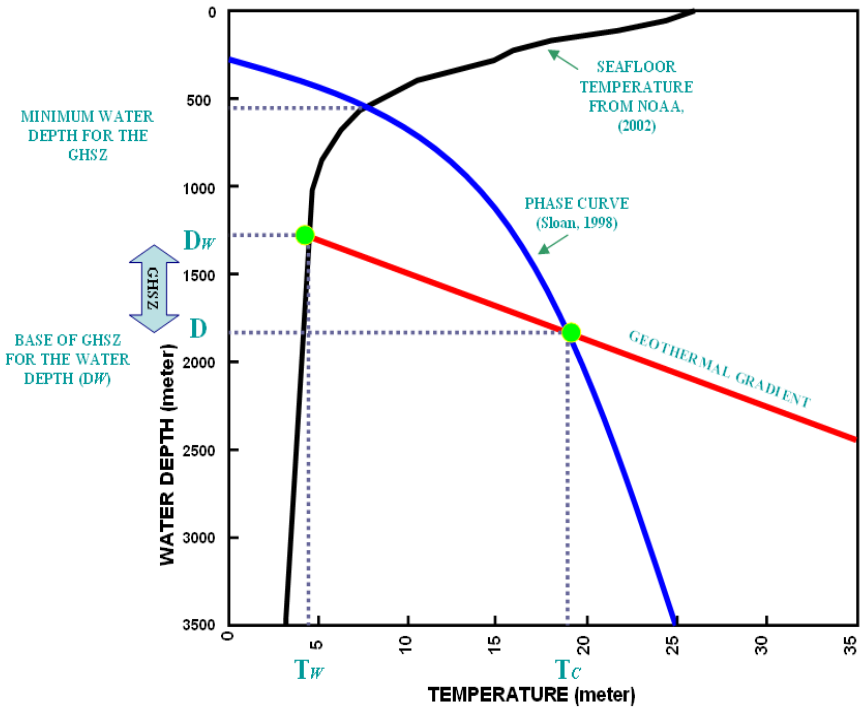

Figure 2. GHSZ thickness. The phase curve (blue line) represents the boundary between the solid phase (stable) and the dissociated phase (unstable) of gas hydrate accumulations (Sloan, 1998). The black line is seafloor temperature as function of water depth appropriate for the Gulf of Mexico (Schlumberger, 2003). The minimum water depth for stable gas hydrate is where this curve intersects the phase curve. The red line represents the temperature increase with depth in the sediments. The base of the hydrate stability zone is at a depth D, where the geotherm intersects the phase curve, and the total thickness of the GHSZ is simply $D-D_w$.

In deep-water, the conventional indication of gas hydrate is the presence of a bottom simulating reflector (BSR) (Kvenvolden, 1993; Cooper and Hart, 2003; Dai et al, 2004). The reflection is generated by a strong acoustic impedance contrast between gas hydrate and free gas host formations at the base of GHSZ (Kvenvolden, 1993; Cooper and Hart, 2003; Dai et al, 2004). The high accumulation of free gas in these formations is due to the trapping of rising gas by gas hydrates above. There are many factors and conditions that define the concentration of gas hydrate within GHSZ, including water depth,

sediment type, temperature, pressure, pore-fluid salinity, gas availability, and gas composition. Moreover, gas hydrate accumulation and concentration can be affected by the local structure, stratigraphy and lithology (Milkov and Sassen, 2001; Lerche and Noeth, 2002; Ruppel et al., 2005).

The purpose of this study is to consider simplified models for predicting the base of the GHSZ in the presence of salt. The predicted depth can then be compared to a regional grid of seismic reflection data in the Gulf of Mexico to better determine which areas may show evidence for gas hydrate. This will allow for a better estimation of the potential volumes of hydrate in the region.

The main focus areas are the Garden Banks and Keathley Canyon regions, which are located 300 km offshore Louisiana and Texas and cover an area of approximately 45,000 square kilometers (Figures 3 and 4). The area is located in the middle of Gulf of Mexico hydrocarbon province where gas hydrate is likely to occur.

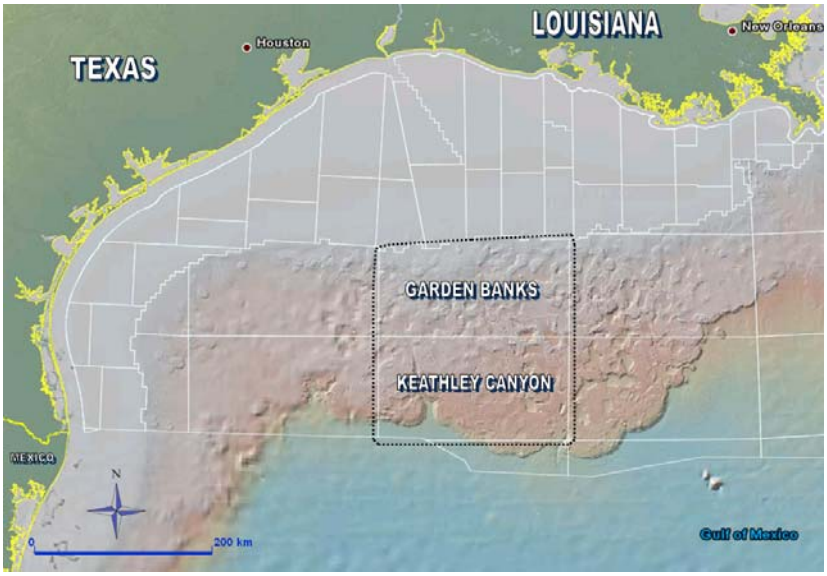

Figure 3. Bathymetry of northwestern Gulf of Mexico. The white lines are the Minerals Management Service (MMS) protraction boundaries. The area of study (square box outlined by-dotted line) covers Garden Banks and Keathley Canyon areas in the Gulf of Mexico outer continental shelf (after Minerals Management Service, 2005).

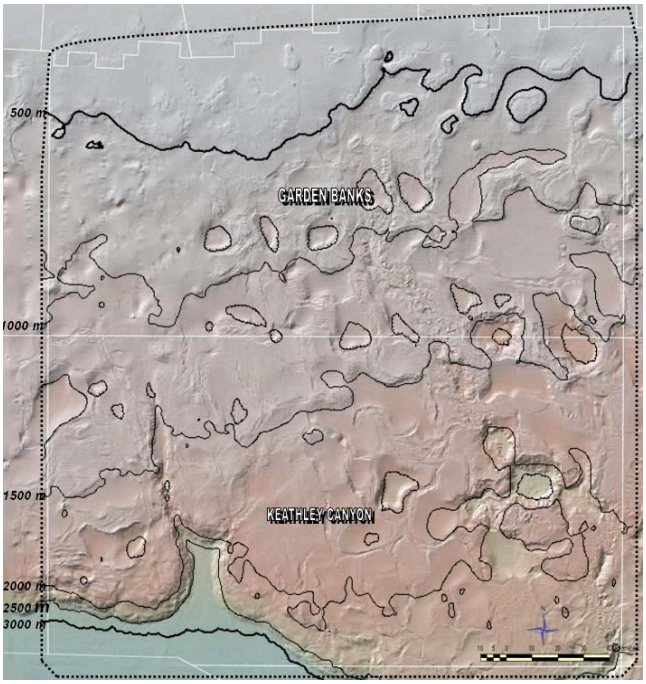

Figure 4. Bathymetry of Garden Banks and Keathley Canyon areas. Black solid lines are bathymetric contours. Seafloor topography shows minibasins and canyons bounded by uplifted salt.

The study is divided into two major steps: (1) a structural interpretation and analysis of sub-seafloor structures; and, (2) an evaluation and estimation of gas hydrate occurrence in the area. The first step is crucial for characterizing the environment where gas hydrate may occur and the impact of these structures on the presence of gas hydrate. This step involves mapping the top-salt and major faults to establish the sub-seafloor structure. The structural interpretation is important for understanding the distribution of salt in three dimensions. The second step is to model the thermal and chemical impact of shallow salt and associated faulting on the possible occurrence of gas hydrate. An existing model of geothermal gradient versus water depth by Milkov and Sassen (2001) is modified by adding the depth of top-salt below seafloor as an additional variable.

2. BACKGROUND

2.1 The Gulf of Mexico - Geologic History and Tectonics

The Gulf of Mexico is an ocean basin that formed during a Late Jurassic continental breakup event that separated the Yucatan Peninsula from the Texas, Louisiana, and Florida coasts (Salvador, 1987; Jacques and Clegg, 2002) (Figure 5). The rifting resulted in thinned basement with an undulating topography. During the Callovian, a thick evaporite layer, the Luann Salt, was deposited (Salvador, 1987). Initially, this occurred in many unconnected basins that eventually merged into a single large salt basin prior to any significant salt deformation or mobilization (Hall, 2002).

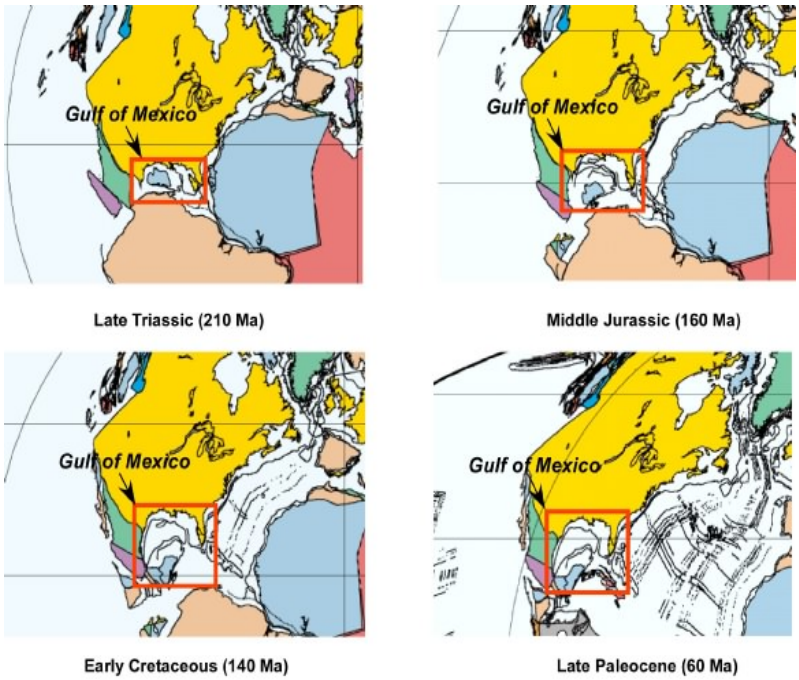

Figure 5. Tectonic evolution of the Gulf of Mexico. The reconstructions here are from Late Triassic through Late Paleocene. The Gulf of Mexico opened during Late Jurassic. Reconstructions are from Lawver et al. (2002).

By the Early Cretaceous, carbonate platforms formed along the margins of the salt basin (Ray, 1988). Erosion took place during the Middle Cretaceous leaving a vast regional unconformity (Ray, 1988). During the Cenozoic, the Mississippi River was established as the major supplier of sediments to the Gulf of Mexico (Ray, 1988). More than 6000 m of continental sediments were deposited on the shelf (Ray, 1988). The Cenozoic stratigraphy changes seaward from thick continental, lagoonal, and deltaic sandstones to inner neritic alternating sands and shales; and, finally, to thick outer neritic and abyssal shales and turbidites (Ray, 1988). The rapid accumulation of Cenozoic sediments resulted in the deformation of the underlying Mesozoic salt. The mobilization of the salt further resulted in faulting, fault-bounded folding, and the formation of minibasins in the overlying formations (Bryant et al., 1990). Generally, the salt tectonics resulted in a complex stratigraphy and a complex fluid and thermal flow system (Trudgill et al., 1999).The recent geomorphology of the deep-water northwestern Gulf of Mexico is characterized by abundant circular or elliptical minibasins that resulted from salt withdrawal and are surrounded by steep slopes and flanked by salt walls (Milkov and Sassen, 2001; Cooper and Hart, 2003).

2.2 Seafloor Depth and Temperature

Figure 4 shows the general distribution of water depths over the area. Most of the northern Garden Banks is shallower than 800 m while part of southern Garden Banks and northwestern Keathley Canyon is within 800-1600 m water depth range. Eastern

Keathley Canyon is characterized by 1600-2500 m water depths. Water depths increase dramatically from 2000 to 3000 m in southwestern Keathley Canyon resulting in the well-known Sigsbee Escarpment. Since water depth is a major factor that determines gas hydrate occurrence, different gas hydrate systems are expected in these major seafloor depth ranges. Seafloor topography shows many local variations in water depth in terms of uplifted areas surrounding flat plains or abruptly alternating with deep canyons. The area is relatively far from the coast (around 300 kilometers) closer to the center of Gulf of Mexico basin and does not show major deep-seated folding systems. Therefore, the relatively lower depths are due to salt tectonism which resulted in uplifted walls of salt bodies surrounding minibasins variable in geometry.

Seafloor temperatures decrease smoothly from 23 to 5°C within the 60-750 m water depth range, which covers northern Garden Banks, while the area deeper than 750 m has temperatures of only 5°C (Figure 6). Thus, the shallow sediments in northern Garden Banks are unsuitable for gas hydrate, while there is a high probability of gas hydrate occurrence in areas of deep and cold seafloor throughout the southern region of the study area.

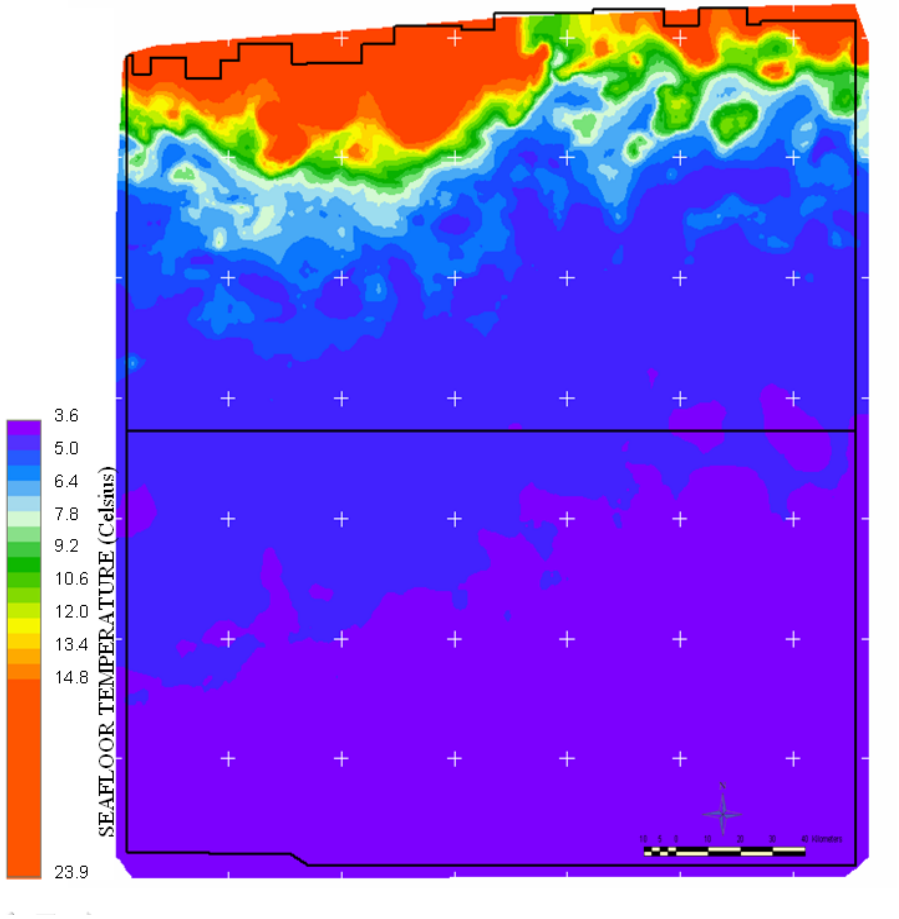

Figure 6. Map of seafloor temperatures in Garden Banks and Keathley Canyon derived from the curve of seafloor temperature vs. water depth (Schlumberger, 2003) (Figure 2). Seafloor temperatures are mostly around 4-5°C in deep-water areas. Seafloor temperatures are mostly around 13-20°C in shallow water areas (less than 500 m deep) (See Figure 4 for water depths).

2.3 Gas Hydrate in the Gulf of Mexico

Gas hydrates were first predicted in the Gulf of Mexico in 1979 based on the identification of key seismic reflections (Shipley et al., 1979). In 1983, samples of gas hydrate were recovered in cores in Green Canyon area (Brooks et al., 1984). Samples of shallow gas hydrates have since been recovered from other locations in the northwestern Gulf of Mexico (Hutchinson et al., 2008)

In terms of temperature and pressure conditions where gas hydrate should be stable, the deep-water Gulf of Mexico should have high potential for large abundances (Hutchinson et al., 2008). Many studies have been conducted to investigate this, resulting in regional maps of expected gas hydrate occurrence (Milkov and Sassen, 2001; Watkins and Buffler, 1996). A major challenge is the deformation caused by salt tectonism (Bryant et al., 1990; Jacques and Clegg, 2002). Salt intrusions and associated faults affect the geothermal gradient in shallow sediments, thereby the GHSZ (Ruppel et al., 2005). Moreover, the stratigraphy of shallow sediments is complicated due to faults, mass wasting, gas chimneys, over-pressured gas zones and geo-pressured shallow sediments (Heggland et al., 2004). The complex lithology also complicates the chemical systems that develop in the regional fluid flow system (Lowrie et al., 1997). Many of these factors decrease the likelihood of concentrated gas hydrates (Ruppel et al., 2005). Moreover, they reduce the likelihood that BSRs may develop even if hydrate is present (Ruppel et al., 2005; Hutchinson et al., 2008). For example, no BSRs were detected in high-resolution seismic reflection data acquired by the U.S. Geological Survey (USGS) from the northern Gulf of Mexico to study gas hydrate as a geo-hazard to deep-water drilling. Instead, high reflectivity zones (HRZs) were observed in the vicinity of faults and salt diapirs below the estimated base of GHSZ. These HRZs were inferred to be free gas formations, above which gas hydrates might be expected.

McConnell and Kendall (2003) suggested that an unconventional type of BSR may indicate gas hydrates in Walker Ridge (east of Keathley Canyon). There, laterally connected, discontinuous high-amplitude anomalous reflections dim out in an up-dip

direction. They interpret the anomalous reflections as trapped free gas and the dim-out as gas hydrates. The individual reflections run parallel to strata but the assembled "BSR" crosscuts strata. These BSRs correlated well with crosscutting reflections in high-resolution 2D sections and are not likely stratigraphic traps.

Dai et al. (2004) discussed the detection and estimation of gas hydrates in Keathley Canyon and Atwater Valley areas. They proposed a workflow that appears to be successful independent of whether or not a BSR is observed. Their approach incorporates high-resolution seismic data that is pre-stack time migrated with an amplitude preserving algorithm, detailed stratigraphic interpretation to identify areas with potential hydrate, seismic attribute analysis to better define the anomalous areas, full waveform inversion for acoustic properties, and finally integrating the results with a rock physics model to estimate the quantity of hydrate present. By using seismic reflection strength, a BSR was definable by terminations of high amplitude gas sands. The interpreted BSR was discontinuous, however. Thin sandy gas bearing sediments with gas hydrate bearing sediments acted like a seal for free gas. These sediments were separated from finer sediments where the BSR is missing.

Frye (2008) developed and applied a model for the assessment of potential gas hydrate reservoir in the Gulf of Mexico outer continental shelf. This study only considered biogenically sourced gas hydrates. Thermogenic gas hydrate evaluation was avoided due to the complexity and poor constraints on deep thermogenic methane generation and migration. Gas hydrate was predicted to accumulate in sandstone reservoirs, shales and fracture reservoirs within the GHSZ. A total volume of around

$314.7x10^{12}$ cubic meters of biogenically produced in-place gas hydrates was estimated in the region. The primary accumulation sites were near mimibasin margins and in front of Sigsbee Escarpment.

2.4 Gas Hydrate Stability Zone Models

The gas hydrate stability zone (GHSZ) is where temperature and pressure are suitable for the crystallization of water and methane into stable hydrate. Temperatures with depth where gas hydrate is stable are determined by a phase curve (Figure 2), which defines the boundary between the stable and unstable phases of gas hydrate. Accordingly, the upper boundary of the GHSZ is in practical terms the seafloor. The lower boundary is the depth below seafloor above which hydrate is thermally stable (solid phase) and below which hydrate is thermally unstable (gas and water). This lower boundary is referred to as the base of the GHSZ. Temperature at the base of the GHSZ is determined from seafloor temperature by the geothermal gradient in shallow sediments, which can be defined based on sediment type and water depth. Defining the thickness of the GHSZ is crucial in estimating the volume of the potential gas hydrate reservoir. Milkov and Sassen (2001) accomplished this using factors derived from only water depth. However, given the presence of shallow salt in the northwestern Gulf of Mexico, the geothermal gradient in shallow sediments is also a function of shallow salt depth and its thermal and chemical impact. Therefore, the Milkov and Sassen (2001) model should be modified accordingly.

Milkov and Sassen (2001) calculated the thickness of the GHSZ and the volume of the gas hydrate reservoir Garden Banks area and the region to the east (water depths around 500-1800 m). They estimated a volume of around two to three trillion cubic meters of hydrate methane at standard temperature and pressure based on the relationship between geologic setting, water depth and GHSZ thickness. However, the thermal impact of shallow salt was ignored due to the lack of a reliable top-salt map and the complexity of modeling the salt impact.

Estimating the geothermal gradient in shallow sediments is one of the most challenging steps for constraining the GHSZ thickness. There is little information about the regional deep heat flow (Jones et al., 2003; Forrest et al., 2005). However, the geothermal gradient has been measured in shallow sediments in a few locations. Because of the complexity of structures in the area, especially the presence of shallow salt bodies and faults, these measurements may be not representative of the geothermal gradient in the whole area. Nevertheless, Milkov and Sassen (2001) derived a general relation between the geothermal gradient and water depth based on the observation that shallow water sediments are usually of higher geothermal gradients than deep-water sediments. According to Milkov and Sassen (2001), the geothermal gradient (G_m) (degree Celsius per meter) in sediments below a seafloor of depth D_w (meter) is

$$G_m = -0.0096 \times \ln(D_w) + 0.0884 . \quad (1)$$

They also derived three phase curves for different methane percentages in gas composition assuming a linear hydrostatic gradient of 10 MPa/km in water and sediments column and a pore fluid salinity of 0.035%. Based on these factors and following the chart in Figure 2, they developed a GHSZ thickness based only on water depth. The calculated GHSZ thickness combined with hydrate concentrations was used to estimate the volume of gas hydrate reservoir in their area of study.

Using the Milkov and Sassen (2001) geothermal gradient model in Equation 1, the phase curve in Figure 2 and the seafloor temperatures in Figure 6, the GHSZ thickness was calculated in Garden Banks and Keathley Canyon (Figure 7). This GHSZ thickness is mostly a function of water depth. This is evident from the similarity between variations in GHSZ thickness and the bathymetry. In general, a thin GHSZ is predicted in shallow water while a thick GHSZ is predicted in deep-water.

A major limitation of the Milkov and Sassen (2001) approach is that the geothermal gradient (Equation 1) is only a function of water depth. The influence of salt on the thermal structure is ignored.

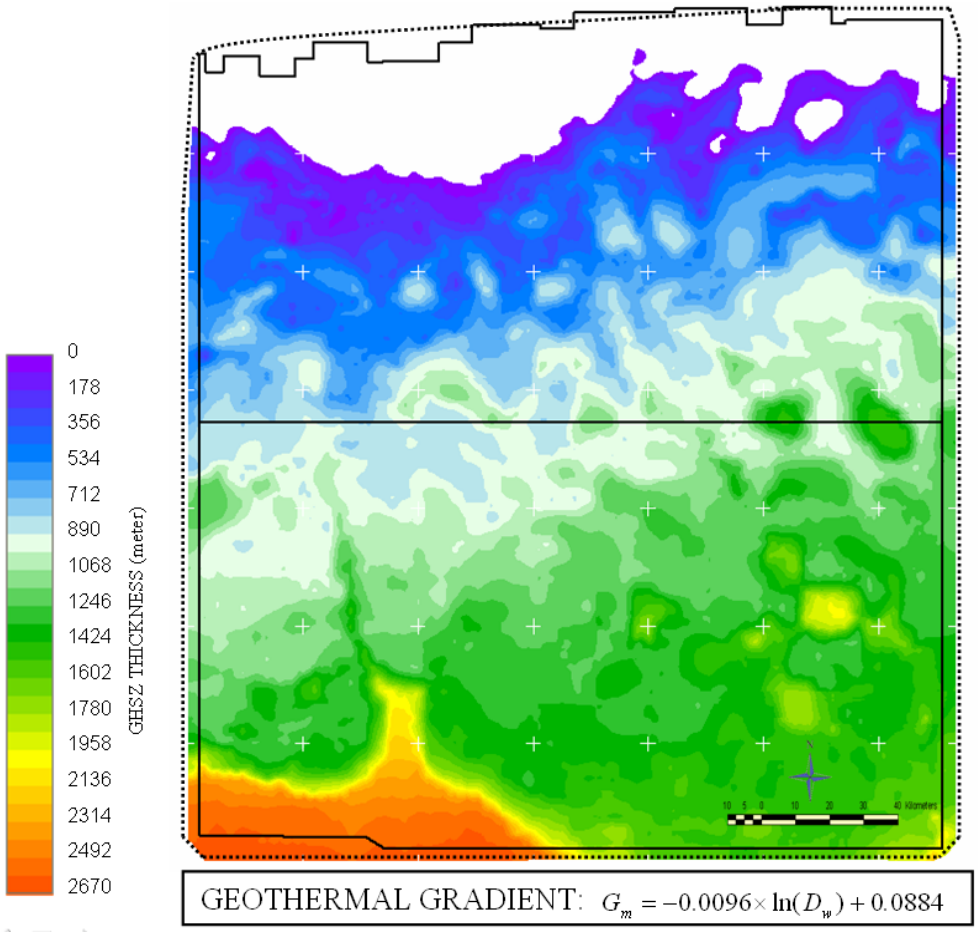

Figure 7. Map of the thickness of the GHSZ based on the geothermal gradient model of Milkov and Sassen (2001). The geothermal gradient model is based on only water depth changes. The geothermal gradient decreases logarithmically with water depth. The resultant GHSZ is thick in deep-water areas and thin or absent in shallow-water areas. This model is the basis for our shallow salt corrected model to estimate the geothermal gradient in shallow sediments.

The presence of shallow salt, which has a strong impact on the thermal structure, is known in the area from many studies (e.g. Watkins and Bufller, 1996; Hall, 2002;. Yu et al, 1992). Salt has a high thermal conductivity and focuses heat flow, producing a positive temperature anomaly in overlying sediments. Thus, sediments over salt that might otherwise be within the GHSZ could be too warm for stabile hydrate. Thus, the

geothermal gradient in shallow sediments should be estimated based on proximity to salt as well as the water depth. To do this, the top-salt must be mapped throughout the area.

In addition to ignoring the thermal impact of salt, Milkov and Sassen (2001) also neglect the impact of the immediate presence of salt within the GHSZ. Figure 8 shows the volume of shallow salt and/or sub-salt sediments included in the GHSZ calculated based on the Milkov and Sassen (2001) model (Equation 1). The thickness of shallow salt and/or sub-salt sediments is high (around 1000 m) in deep-water areas (thick GHSZ). This shallow salt volume should be excluded from GHSZ.

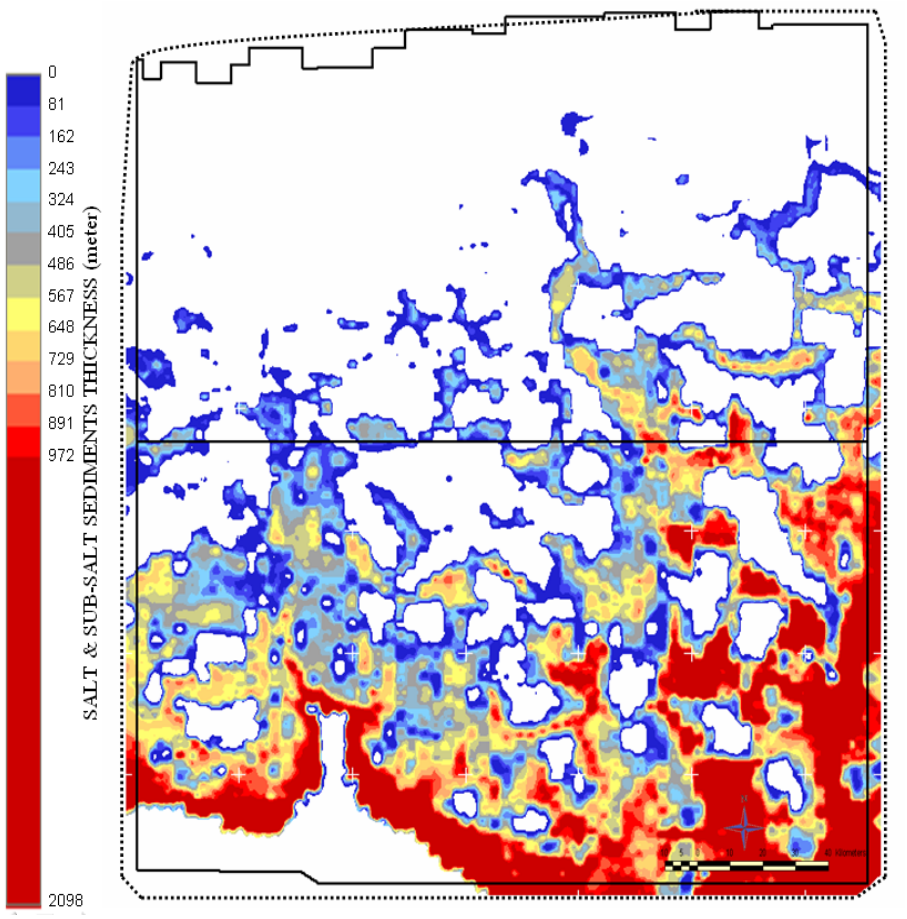

Figure 8. Map showing the thickness of salt and/or sub-salt sediments included in the GHSZ calculated based on the geothermal gradient model by Milkov and Sassen (2001) (Figure 7).

3. METHODS

3.1 2D Seismic Data

A large volume of data exist over most of the northern Gulf of Mexico where gas hydrates are likely to occur (Cooper and Hart, 2003; Hutchinson et al., 2008). Over several decades, TGS-NOPEC has acquired thousands of kilometers of 2D data covering the northwestern Gulf of Mexico (TGS-NOPEC, 2004). In this study, data from two 2D seismic surveys were used. The Phase 20 survey covers the northern Garden Banks and the Phase 30 covers the southern Garden Banks and Keathley Canyon areas (Figure 9, TGS-NOPEC, 2004). Both surveys recorded to 7 seconds two way travel time.

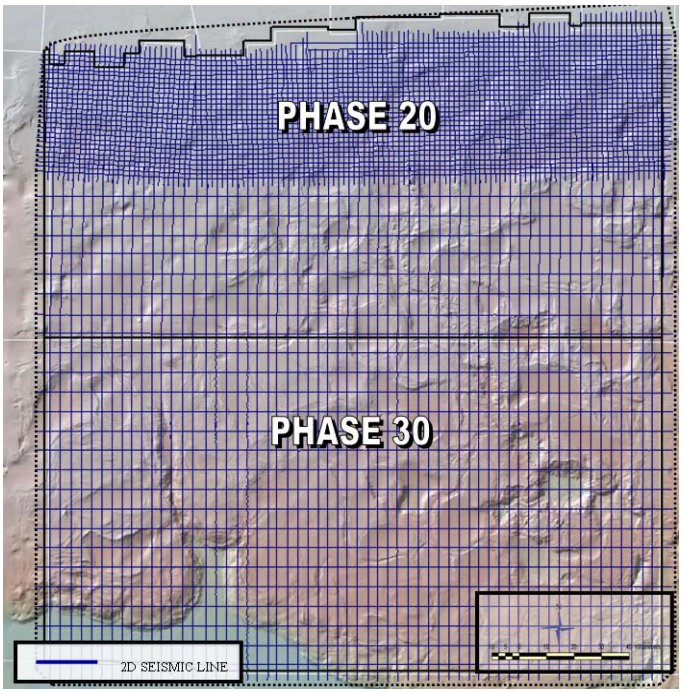

Figure 9. Grid of 2D seismic data lines used in this study. The data were acquired by TGS-NOPEC in 1986.

3.2 Sub-seafloor Structure Mapping

The top-salt was mapped along 2D lines. Throughout the area, the top-salt is observed as a strong reflection below which reflections are absent or imaging is very poor. In general, the imaging through the salt is too poor to map the bottom of salt. Because of this, it is hard to identify the true geometry and thickness of salt bodies. Salt layers may be as thick or thicker than 5000 m in the center of salt diapers. In contrast, salt may have a thin or zero thickness in pinch-out areas where salt has been partially or completely withdrawn (very thin salt sheets and/or salt welds). In this study, salt welds are mostly mapped to connect thick salt bodies. In cross sections, they were mapped through stratigraphic boundaries where noticeable changes in dipping strata mark the base of minibasins between shallow salt bodies. In this study, we further assume that all sediments below base salt are unable to host gas hydrate. Thus, the placement of salt welds can influence final hydrate volume estimates. In general however, the salt welds are mostly deep enough (4000-5000 m below seafloor) that their impact is minimal.

From the top-salt map, it is possible to define minibasins based on the distribution of shallow salt bodies. Shallow salt tends to concentrate into attached or closely spaced salt bodies resulting in salt walls that range in length from a few kilometers to tens of kilometers. These salt walls surround minibasins where sediments are thicker than 500 m in the interior. The boundaries that separate these minibasins are drawn through the picks of the bounding shallow salt bodies.

The interpreted minibasins represent areas with relatively homogeneous

stratigraphic patterns normally consisting of horizontal or slightly dipping strata. Strata in neighboring minibasins dip in opposite directions away from the top of shallow salt.

In addition to mapping the top-salt and associated mini-basins, we mapped the areas where shallow-rooted fault planes are spaced less than one kilometer along a 2D seismic line. These zones, which mark areas of significant deformation, were first constructed on individual 2D seismic lines then interpolated throughout the area.

The seafloor was mapped using the 2D seismic sections. The two-way travel time values were depth converted using a water velocity of 1500 m/sec. Seafloor depths were interpolated between the 2D lines and seafloor temperatures were predicted based on the seafloor temperature vs. water depth curve of Schlumberger (2003, Figure6).

To calculate the effect of the salt on the hydrate stability zone, we also require depth estimates to the top salt. This is difficult since there are no velocity data available and only scattered well data. To estimate depth, we assume a simple constant velocity of 2000 m/sec through the sediments to top salt.

3.3 Gas Chimney and BSR Detection

Gas chimneys were detected by the following characteristics (Schlumberger, 2003):

- Reflections in gas chimneys are blurred due to the presence of free gas.

- Reflections close to gas chimneys are shifted down due to low velocities inside the gas chimney.

- Gas chimneys are often manifested on the seafloor as hydrate mounds, which are easily detected in seismic sections.

In general, gas chimneys that reach the seafloor are expected in greater abundance in areas where the seafloor is shallower than the upper boundary of GHSZ. In these areas, free gas is not trapped by crystallizing into gas hydrates or being blocked by the already existing gas hydrates.

BSRs were distinguished from the background stratigraphy by several distinctive properties (Dai et al., 2004; Snyder et al., 2004; Bünz et al., 2005):

- BSRs are strong reflections due to large acoustic impedance contrast.

- BSRs are phase-reversed compared to seafloor reflection.

- BSRs crosscut stratigraphic reflections.

- BSRs are not displaced by faults, unlike stratigraphic reflections.

- Reflections above BSRs are dimmed-out due to gas hydrate presence.

BSRs and BSR-like phenomena may be observed along the flanks of minibasins as en-echelon reflections that crosscut stratigraphy (Milkov and Sassen 2001; Dai et al., 2004; Snyder et al., 2004; Hutchinson et al., 2008). However, it is important to note that throughout this region, these BSRs are limited and do not simulate the seafloor like conventional BSRs because of the effects of the salt. Next we describe a simple method to calculate the base of the hydrate stability zone that includes the effect of salt to aid in identifying BSRs.

3.4 Geothermal Gradient Calculation

Based on the study by Jensen and Sørensen (1992) and given that salt welds and thin salt sheets are only observed deeper than 4500 m below seafloor, we assumed that salt has its maximum thickness at seafloor and its minimum thickness at 4500 m below seafloor. For simplicity, salt thickness between these two depths below seafloor is assumed to be linear with depth below seafloor.

Based on the Yu et al. (1992) study, the temperature anomaly at the top-salt is proportional to salt thickness. Where observed in the Gulf of Mexico, salt produces a maximum temperature anomaly of around 30°C when it is very thick, > 5000m (Yu et al., 1992). In the region mapped for this study, salt is only half that thick (Hall, 2002). Thus we limit the temperature anomaly to be 15°C, which in practical terms results in thermal gradients less than 0.1°C/m. In addition, salt can not cause any temperature anomaly if it is deeper than 4500 m below seafloor (i.e. 0°C temperature anomaly). For simplicity, we assume that the top-salt temperature anomaly vs. top-salt depth below

seafloor between these two boundaries is linear (Figure 10). Therefore, the temperature anomaly (ΔT) (degree Celsius) that a salt body of depth D_{sw} below seafloor is

$$\Delta T = -0.0035 \times D_{sw} + 15 . \quad (2)$$

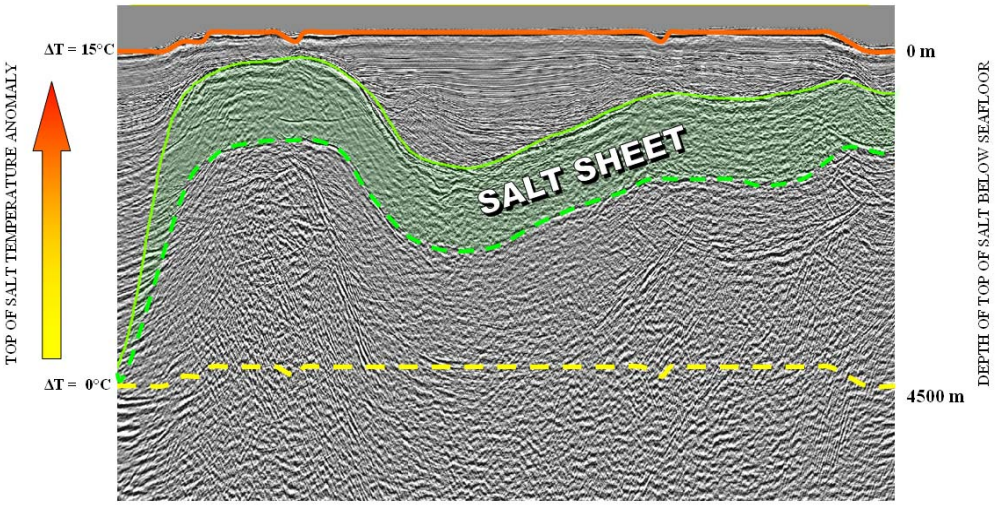

Figure 10. Salt thermal impact model. A schematic demonstration of the top-salt temperature anomaly model and its boundary conditions (Equation 2). Predicted temperature anomaly at the top-salt is 0°C at depth 4500 m below seafloor and 15°C at seafloor. The top-salt temperature anomaly vs. top-salt depth below seafloor between these two boundaries is assumed to be linear (Yu et al, 1992; Jensen and Sørensen, 1992).

Using the Milkov and Sassen (2001) geothermal gradient model (Equation 1), the temperature at the top-salt without the thermal impact of salt (T_{ms}) (degrees Celsius), given a seafloor temperature of T_w (degrees Celsius), is

$$T_{ms} = G_m \times D_{sw} + T_w , \quad (3)$$

or (from Equation 1),

$$T_{ms} = [-0.0096 \times \ln(D_w) + 0.0884] \times (D_{sw}) + T_w . \quad (4)$$

By adding the temperature anomaly that salt can cause at its top ($\boldsymbol{\Delta T}$) (Equation 2) to the temperature at the top-salt without the thermal impact of salt (T_{ms}), temperature at the top-salt (T_s) (degree Celsius) is

$$T_s = T_{ms} + \Delta T \ . \quad (5)$$

Subsequently, the geothermal gradient in shallow sediments will be adjusted given the new calculated temperature at the top-salt (T_s). The new shallow salt thermally corrected geothermal gradient (G) (degree Celsius per meter) will be

$$G = \frac{T_s - T_w}{D_{sw}} . \quad (6)$$

From Equation 5,

$$G = \frac{T_{ms} - T_w + \Delta T}{D_{sw}} . \quad (7)$$

From Equation 4,

$$G = \frac{[-0.0096 \times \ln(D_w) + 0.0884] \times D_{sw} - 0.0035 \times D_{sw} + 15}{D_{sw}}, \quad (8)$$

or finally,

$$G = -0.0096 \times \ln(D_w) + 0.0849 + \frac{15}{D_{sw}}. \quad (9)$$

3.5 GHSZ Thickness Calculation

Based on the new geothermal gradient model (Equation 9), GHSZ thickness was calculated using inputs and steps shown in Figure 11.

The phase curve is the equation that defines the stability of gas hydrate given its gas composition in sediments. It is the relation between depth and critical temperature at which gas hydrate may change from a stable phase (solid gas hydrate) to unstable phase (separate gas and water). This relation changes according to the gas composition of gas hydrate (Sloan, 1998), which is variable throughout the area. For simplicity, we ignore this compositional variation and use the curve calculated by Sloan (1998) for a hydrate composed of 100% methane as the gas component (Figure 2). The critical temperature, T_c, at the base of a GHSZ of depth, D, below the sea surface is

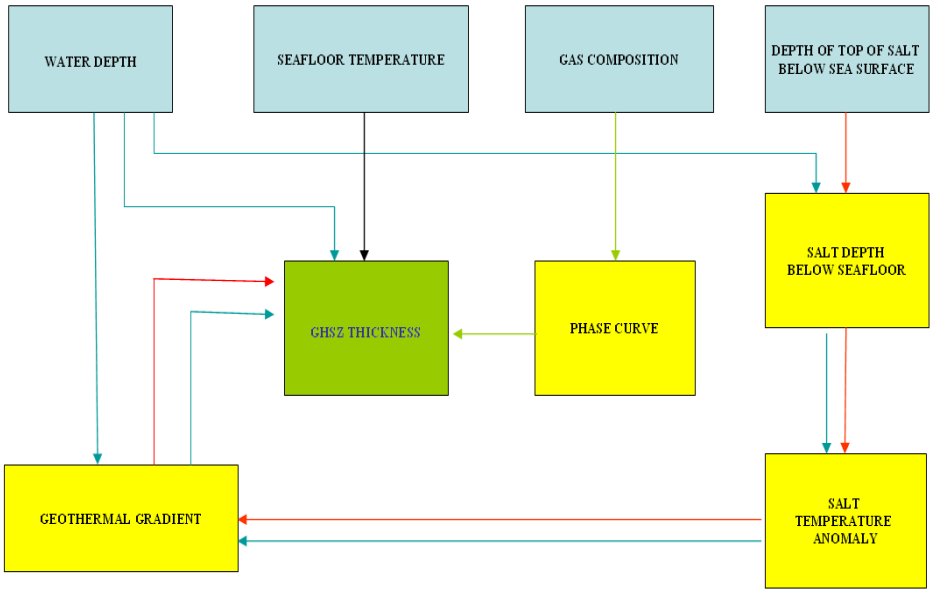

Figure 11. Work flow chart. The chart demonstrates the inputs and steps needed to calculate the thickness of the GHSZ (green box) according to the chart in Figure 2. Blue boxes are the inputs. Yellow boxes are the intermediate outputs. The inputs are (1) water depth (D_w) (blue arrows indicate the contribution of water depth), (2) seafloor temperature (T_w) (black arrow indicates the contribution of seafloor temperature), (3) gas composition from Sloan (1998) (green arrows indicate the contribution of gas composition) and (4) depth of top-salt below sea surface (D_s) (red arrows indicate the contribution of depth of top-salt below sea surface). Phase curve (critical temperature, T_c) is calculated from gas composition and depth of sediments (Equation 9) (Sloan, 1998). Depth of top-salt below seafloor (D_{sw}) is calculated from depth of top-salt below sea surface (D_s) and water depth (D_w). Then, top-salt temperature anomaly is calculated from depth of top-salt below seafloor (D_{sw}) (Equation 2). Geothermal gradient (G) is calculated from top-salt temperature anomaly and water depth (D_w) (Equation 8). Finally, GHSZ thickness is calculated from water depth (D_w), seafloor temperature (T_w), phase curve (critical temperature, T_c) and geothermal gradient (G) (Sloan, 1998) (Equation 17).

$$T_c = 8.9059 \times \ln(D) - 47.907 . \qquad (10)$$

From Figure 2, the upper theoretical boundary of the GHSZ is the maximum water depth where seafloor temperature is higher than the critical temperature for stable gas

hydrates at that depth. This water depth is 550 m in our area, resulting in no or only a thin GHSZ in the northern Garden Banks.

The base of the GHSZ is the depth where the sediment temperature is critical for the stability of gas hydrates. Above this base are sediments that host solid gas hydrate and below are sediments that host free gas. From Figure 2, this depth (D) is where sediments temperature, $T_{d,}$ matches the critical temperature for the stability of gas hydrates, T_c, or

$$T_d = T_c . \tag{11}$$

From Figure 2, T_c is related to T_w through the geothermal gradient (G) or

$$T_d = G \times (D - D_w) + T_w . \tag{12}$$

From Equations 10 and 12,

$$G \times (D - D_w) + T_w = 8.9059 \times \ln(D) - 47.907 . \tag{13}$$

This equation can be solved and the depth of the base of GHSZ below sea surface (D) can be calculated by finding the zero of the function

$$f(D) = G \times (D - D_w) - [8.9059 \times \ln(D)] + T_w + 47.907 . \tag{14}$$

Or from Equation 9

$$f(D) = [-0.0096 \times \ln(D_w) + 0.0849 + \frac{15}{D_{sw}}] \times (D - D_w) - [8.9059 \times \ln(D)] + T_w + 47.907. \quad (15)$$

The thickness of the GHSZ (D_{GHSZ}) is the thickness of sediments between the seafloor and the base of the GHSZ, or

$$D_{GHSZ} = D - D_w. \quad (16)$$

D_{GHSZ} can be directly calculated from water depth, (D_w), sediment thickness above salt (D_{sw}); and seafloor temperature (T_w) by finding the zero of the function

$$f(D_{GHSZ}) = [-0.0096 \times \ln(D_w) + 0.0849 + \frac{15}{D_{sw}}] \times (D_{GHSZ}) - [8.9059 \times \ln(D_{GHSZ} + D_w)] + T_w + 47.907. \quad (17)$$

This can be done using Newton-Raphson's method, a frequently used numerical method in finding the zeros of real-valued functions (Deuflhard, 2004). The resultant GHSZ thickness versus water depth relation is shown in Figure 12.

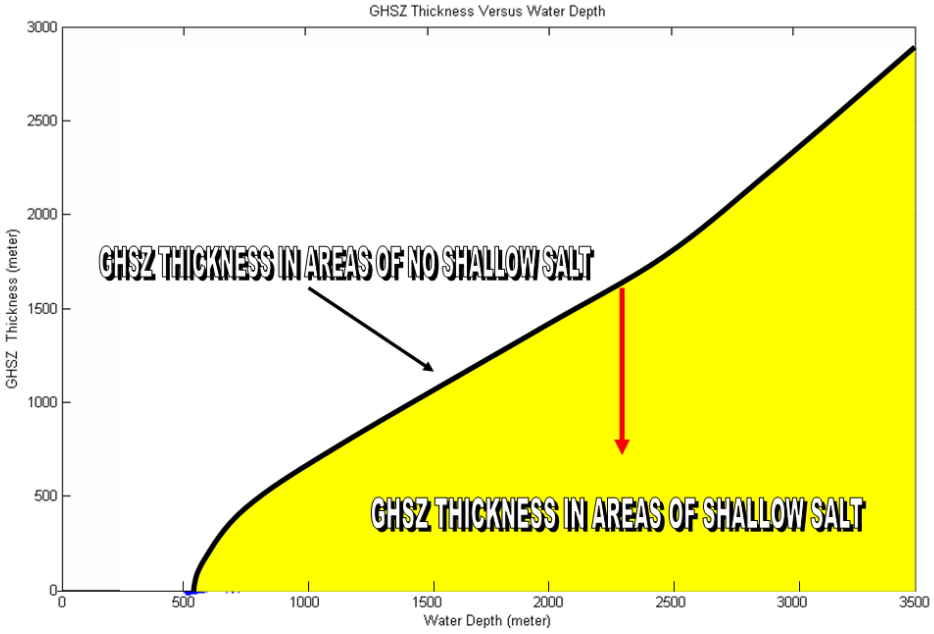

Figure 12. GHSZ thickness vs. water depth. The black line represents the relation in areas with no salt or salt deeper than 4500 m below seafloor. This curve matches the results based on a model developed by Milkov and Sassen (2001). In areas of shallow salt, GHSZ thickness decreases (red arrow) and the curve will shift into the yellow region. The decrease in GHSZ thickness in these areas is proportional to the depth of the top-salt below sea surface. GHSZ thickness vs. water depth takes an irregular shape within the yellow area according to Equation 17.

4. RESULTS

4.1 Sub-Seafloor Structure in Garden Banks and Keathley Canyon

Shallow salt is abundant in the deep-water of northwestern Gulf of Mexico and is one of the most important sources of post-rift deformation in the Gulf of Mexico (Trugill et al. 1999; Watkins et al. 1996). In seismic sections, salt bodies are characterized by irregular patches of transparent zones with a strong top reflection. In the Gulf of Mexico, salt related features alternate with synclines, forming dome and sheet-like structures with steep walls topped by domed caps or irregular surfaces from which faults radiate upward (Watkins and Buffler, 1996) (Figure 13).

Figure 14 shows the detailed depth structure map of the top-salt. Deep salt is usually thin or completely withdrawn (salt welds), whereas shallow salt is typically very thick. Figure 15 is a 3D image of the top-salt. In the northern Garden Banks area, there are fewer shallow salt diapirs compared to the southern region, resulting in larger and deeper minibasins. However, the amount of deformation is high in this area. This is evident in the many deep-seated major faults that connect the salt diapirs. A continuous salt canopy dominates the southern Garden Banks and Keathley Canyon area. A few deep, isolated minibasins are scattered within this massive salt canopy. Figure 16 shows the distribution of shallow salt (less than 950 m below seafloor) and the surrounding minibasins.

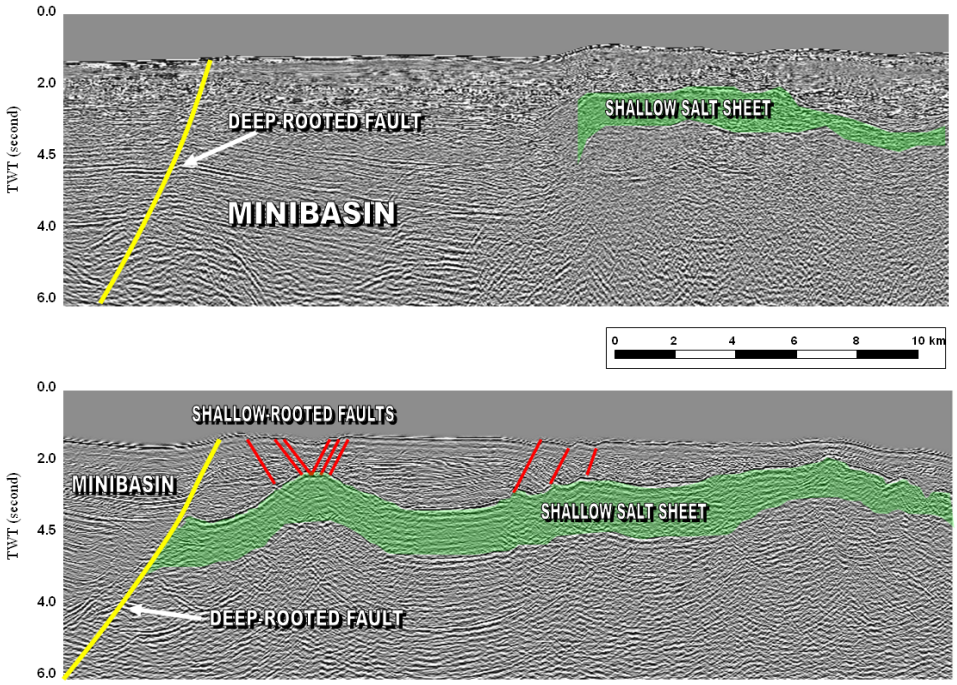

Figure 13. Two interpreted seismic sections showing typical sub-seafloor structures. Green patches are shallow salt sheets. The top-salt is well-defined from seismic reflections while the bottom of salt is predicted based on shallow salt evolution and morphology in the northwestern Gulf of Mexico (Hall, 2002). In most areas, shallow salt was mapped as canopies of wide and thick sheets or closely spaced salt diapirs. Deep-rooted faults (yellow lines) run through minibasin flanks connecting salt diapirs. Sub-salt faults are untraceable (Hall, 2002). Shallow salt related faults (red lines) radiate from the top-salt up to seafloor. They usually cause noticeable displacement on seafloor indicating that they are currently active (Geresi et al., 2002; Hall, 2002).

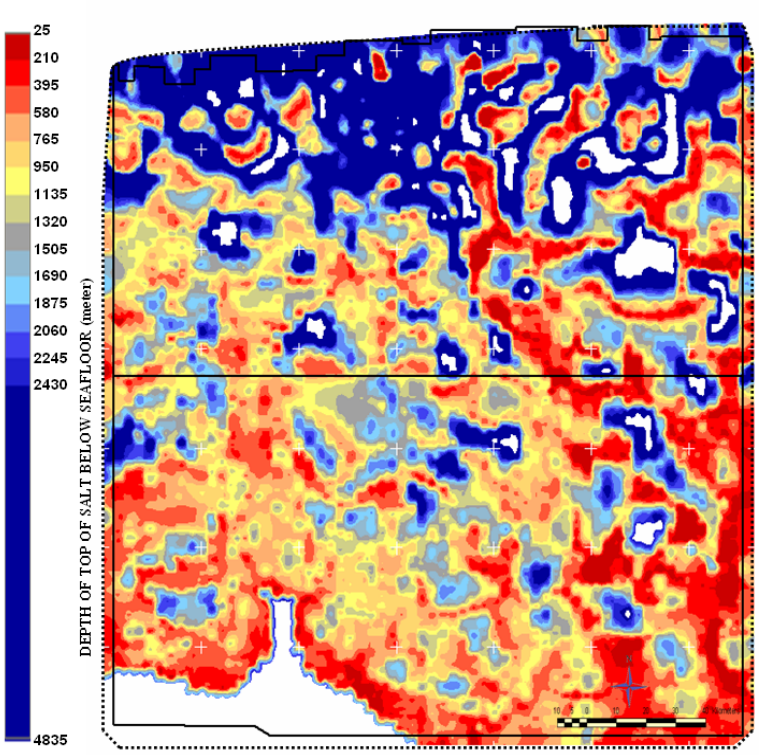

Figure 14. Depth structure map of the top-salt below seafloor. Blank areas are the areas where salt or salt welds are deeper than 5000 m below seafloor. Salt depth below seafloor generally reflects salt thickness.

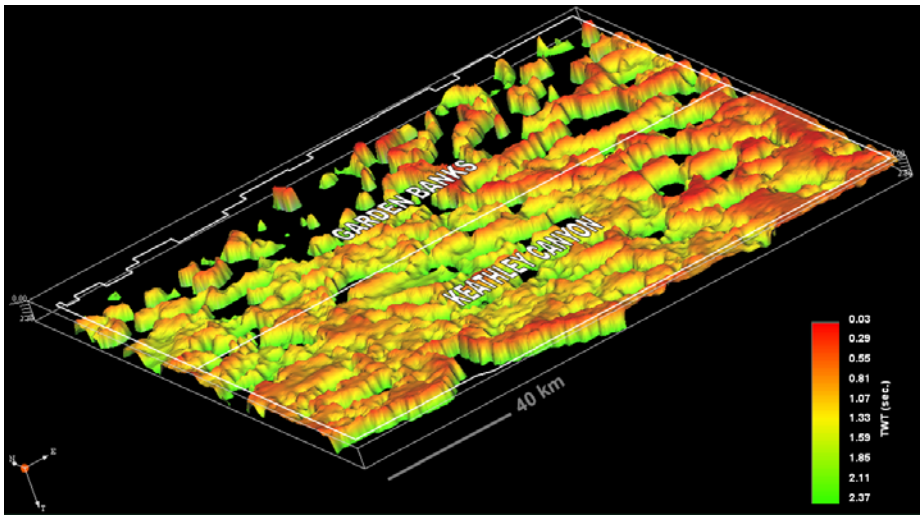

Figure 15. 3D image of the top-salt time structure map. Salt appears more in diapiric patterns in Garden Banks while it appears more in sheet-like patterns in Keathley Canyon. In the southwestern Keathley Canyon area, Sigsbee Escarpment and Keathley Canyon gorge are the result of the advancing salt canopy front (Hall, 2002).

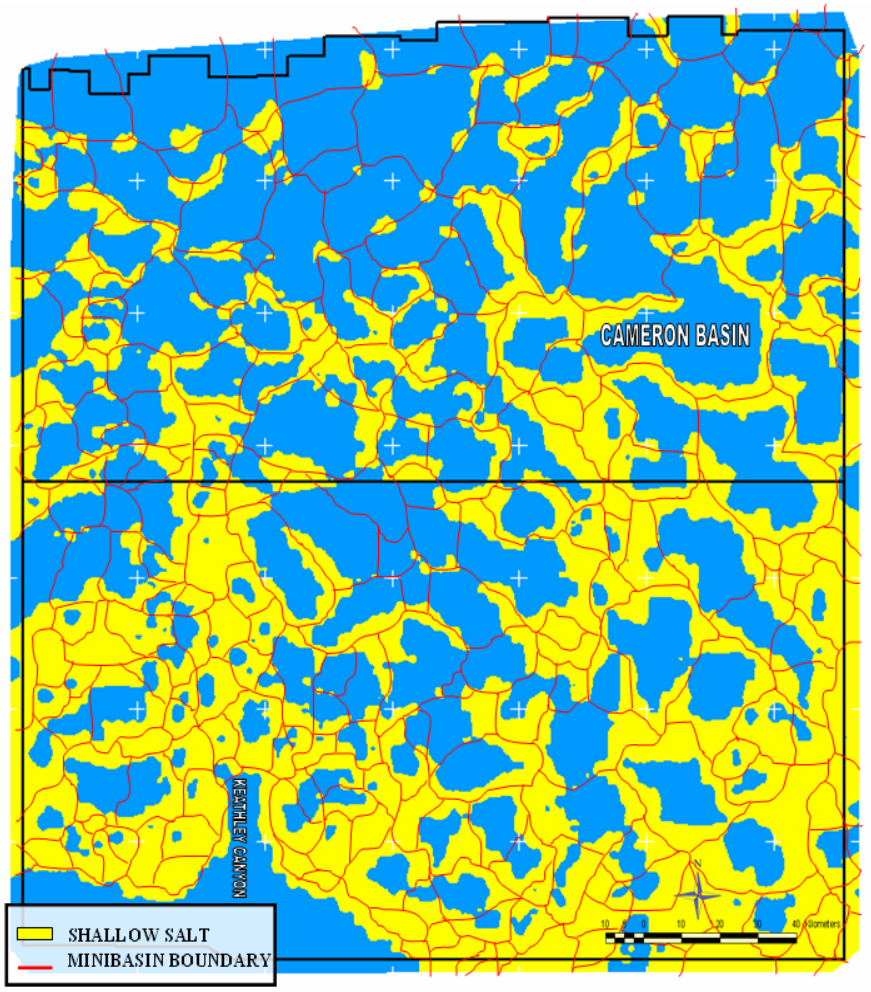

Figure 16. Distribution of shallow salt (yellow) (less than 950 m below seafloor) and major minibasins (blue). The shallow salt defines the flanks of the mini-basins. Large minibasins are underlain by deep salt or salt welds. Many smaller minibasins are underlain by shallow salt (minibasins with yellow interiors). Red lines represent minibasin boundaries or divides through shallow salt picks.

Faults in Garden Banks and Keathley Canyon can be assigned to two categories: (1) deep-seated faults and (2) shallow-rooted faults. In the first category, deep-seated faults appear as major normal faults rooted to more than 1200 m below seafloor. They are usually associated with many smaller synthetic and antithetic faults creating a zone of

deformation that is generally more intense in the hanging wall blocks. These faults are found primarily in the northern central part of Garden Banks (Figure 17).

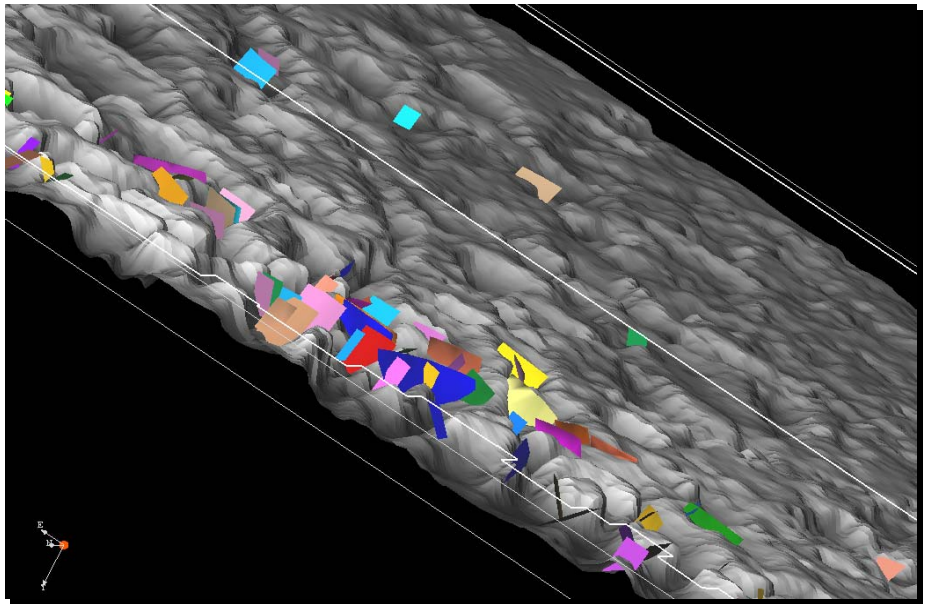

Figure 17. 3D image of deep-rooted faults mapped in the area (colored surfaces). The faults are imposed on the top-salt topography map (gray shaded surface). Deep-rooted faults are mostly clustered in the northern-central part of Garden Banks cutting through the major minibasins and connecting the scattered salt diapirs. To the south, in Keathley Canyon, the large salt canopy covers most of sub-salt deep-rooted faults (Hall, 2002). Deep-rooted faults are possible conduits for the migration of deep thermogenic methane into the shallow GHSZ (McConnell and Kendall, 2003).

In the second category, most shallow formations in the area are deformed by faults that radiate from shallow salt bodies (Figure 13). These are also normal faults but limited in length and displacement. Many of them are traceable to the seafloor. They are often found in clusters that define shallow deformation zones that can be mapped over large areas (Figure 18).

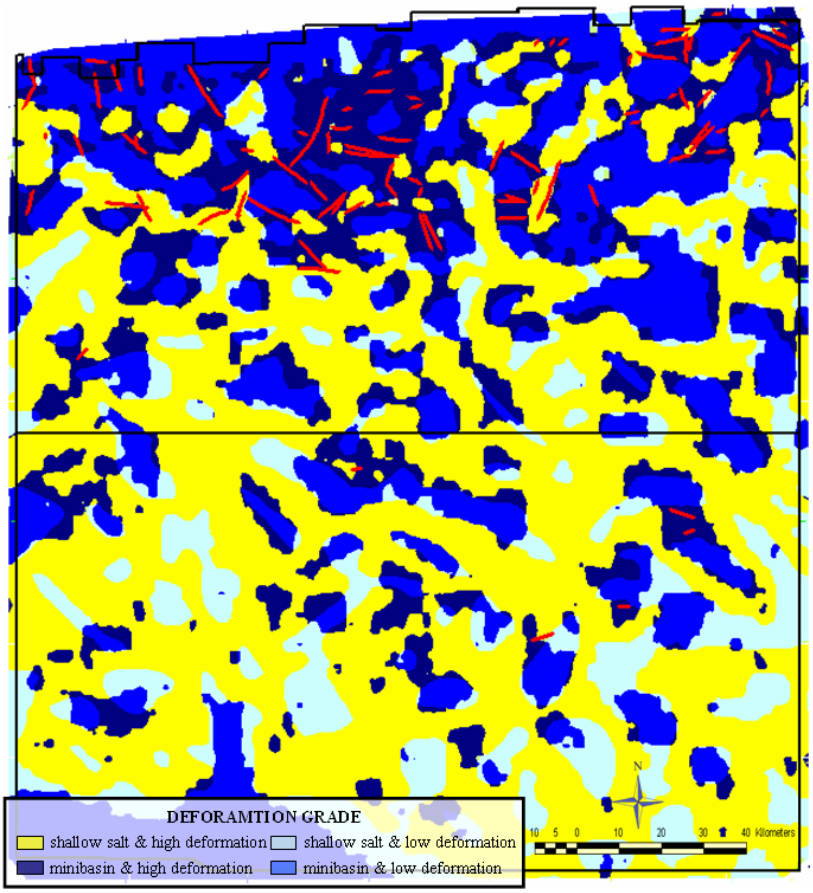

Figure 18. Deformation in shallow sediments. The deformation is in terms of deep-rooted faults and shallow-rooted salt-related faults. Thick red lines trace major deep-rooted faults. Yellow denotes areas of highly deformed shallow sediments overlying shallow salt. Light blue denotes areas of moderately deformed shallow sediments overlying shallow salt (fewer faults). Dark blue denotes areas of highly deformed shallow sediments overlying major minibasin flanks. Intermediate blue denotes areas of moderately deformed shallow sediments in major minibasin interiors.

4.2 Geothermal Gradient and GHSZ Thickness

Using the mapped top-salt (Figure 14), the salt thermal impact model (Equation 3) was used to modify Milkov and Sassen (2001) geothermal gradient model (Equation 1). The inputs and steps of calculating the new geothermal gradient is detailed in Figure 11 and Equations 1-9. The resultant geothermal gradient model is a function of water depth and depth of salt below seafloor (Equation 9). Figure 19 shows the map of the

geothermal gradient in shallow sediments calculated from Equation 9. Geothermal gradient values vary from 0.01-0.04°C/m in the deep-water minibasins and are high as 0.05-0.08°C/m in regions of very shallow salt and shallow water regions.

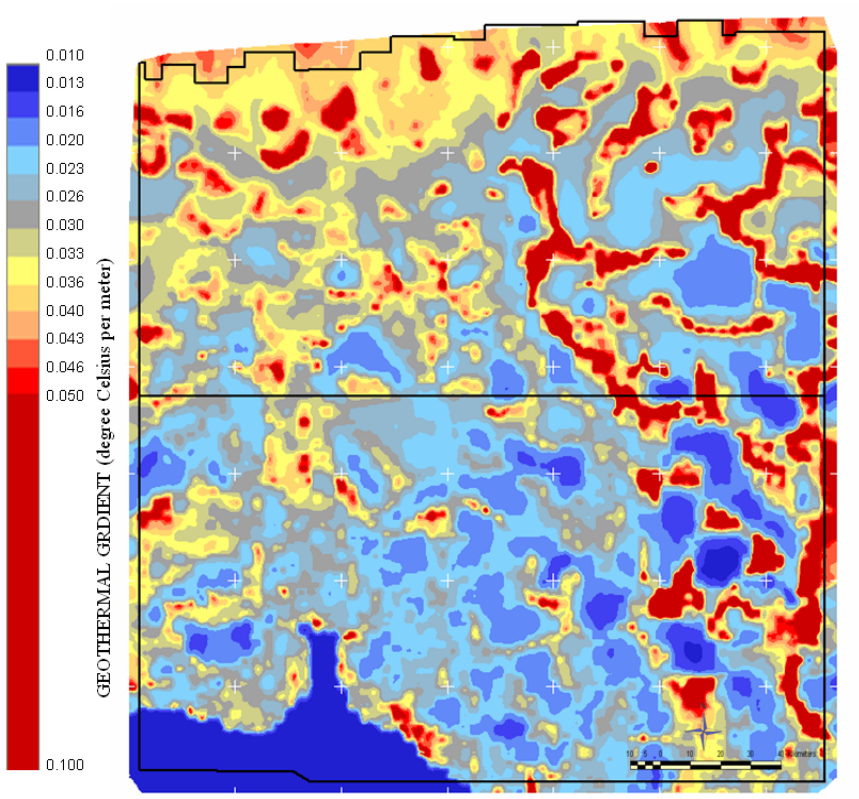

Figure 19. Map of geothermal gradient values in shallow sediments overlying salt. Values of geothermal gradient vary from 0.01-0.04°C/m in shallow sediments of deep-water minibasins to 0.05-0.08°C/m in sediments overlying shallow salt and in shallow water sediments in northern Garden Banks.

Using the inputs and steps detailed in Figure 11 and Equations 10-17, the gas hydrate stability zone thickness was calculated (Equation 17) over the entire study area (Figure 20). This GHSZ map is thus a function of water depth, seafloor temperature, and the depth of top-salt below seafloor.

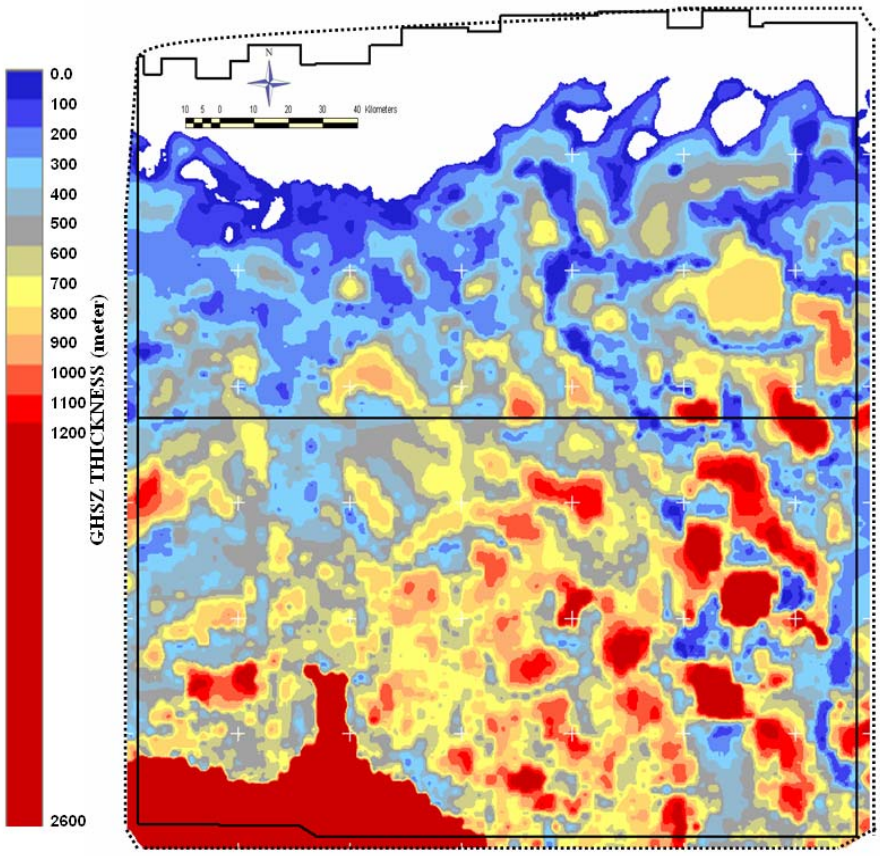

Figure 20. Map of the thickness of GHSZ calculated from Equation 17. This GHSZ thickness is thermally corrected and incorporates the impact of water depth, depth of the top-salt below seafloor and seafloor temperature (Equation 17). GHSZ is thick (around 1000 m) in deep-water areas and in minibasin interiors while thin in shallow water areas and areas of shallow salt (less deep than 1000 m below seafloor). In the northern shallow water areas (less than 500 m deep), GHSZ is absent (Blank area).

In Figure 20, most of the salt volume in Figure 8 is below the base of the GHSZ (Equation 17). Nevertheless, a there remains some small areas where the salt is within the calculated GHSZ. This remnant salt volume is shown in Figure 21.

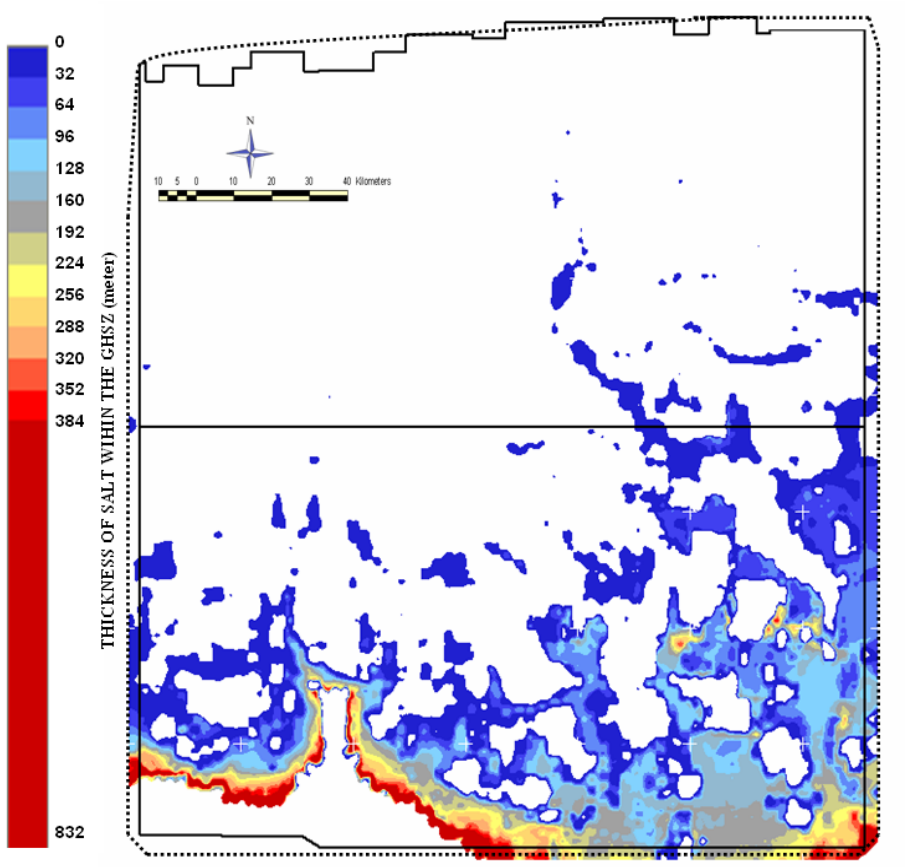

Figure 21. Map of the thickness of shallow salt and/or sub-salt sediments within the thermally corrected GHSZ calculated from Equation 17 (Figure 20).

In terms of pressure and temperature, the salt volume in Figure 21 is still within the thermally corrected GHSZ (Figure 20) but it will have a zero concentration of gas hydrates. Therefore, this volume was simply excluded from GHSZ for estimating the potential volumes of gas hydrate. By subtracting this remaining salt volume from GHSZ, the final GHSZ thickness

$$D_{FGHSZ} = \begin{cases} D_{GHSZ} & if \quad D \le D_s \\ D_{FGHSZ} - D - D_s & if \quad D \ge D_s \end{cases} . \qquad (18)$$

Figure 22 shows the final thickness of the GHSZ (Equation 18). The GHSZ is absent to very thin in the northern Garden Banks. High seafloor temperatures (8-23°C) in these shallow water depths (60-500 m) combined with the high geothermal gradient prevents hydrate from forming. From the southern Garden Banks and southward, the GHSZ thickness increases due to the increasing water depths, decreasing seafloor temperatures, and decreasing geothermal gradient values in deep-water sediments. However, this only applies to the interiors of major minibasins. Shallow salt areas have an anomalously thin GHSZ due to the thermal impact of salt.

Variations in the GHSZ thickness map correlate strongly with the geothermal gradient map (Figure 19) showing that the geothermal gradient is one of the main factors controlling hydrate stability (Figure 2).

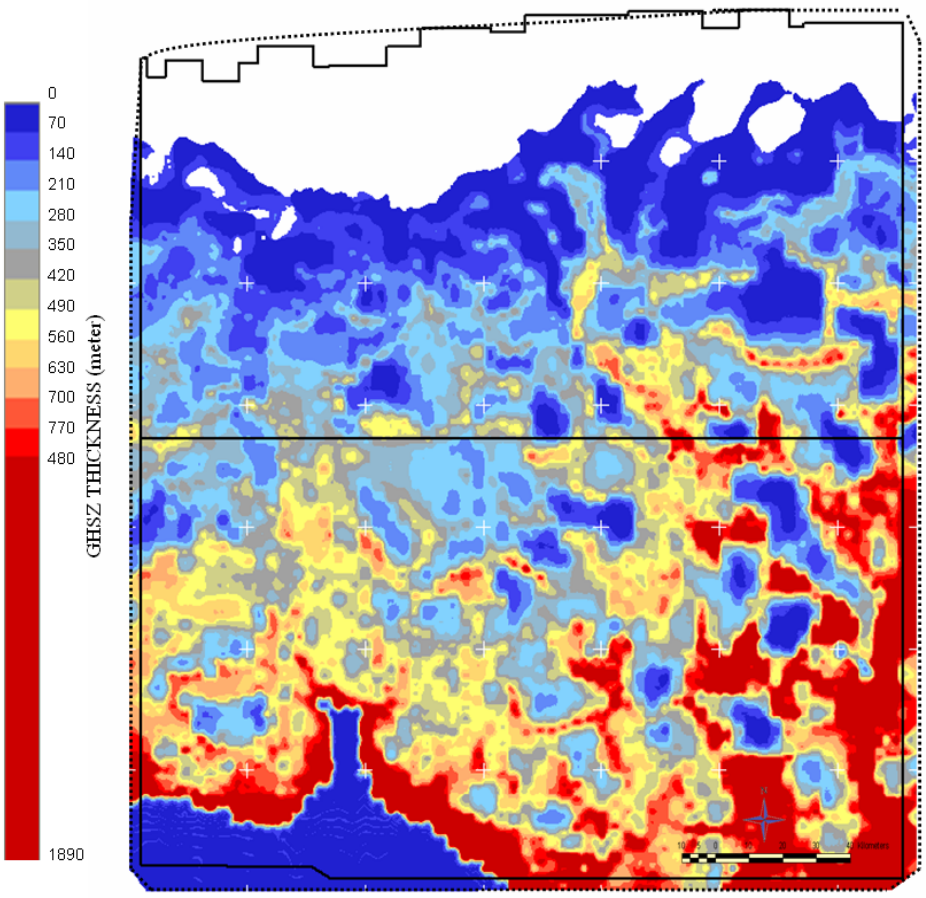

Figure 22. Map of the final thickness of the GHSZ calculated from Equation 18. This GHSZ thickness is thermally and chemically corrected and incorporates the impact of water depth, depth of the top-salt below seafloor and seafloor temperature (Equations 17and 18).

5. DISCUSSION

5.1 Shallow Salt Distribution and Evolution

In the northern Garden Banks, salt diapirs are common (Hall, 2002). The overall structure suggests a thin autochthonous salt layer heavily and quickly depleted by the thick and fast deposition of overburden sediments resulting in massive deformation. This deformed area is a typical place for gas hydrates to concentrate. Unfortunately, water depths in the northern Garden banks are too shallow and thus too warm to develop gas hydrates.

In the southern Garden Banks, thick salt is interspersed with minibasins that develop in response to salt tectonics. These minibasins are smaller and shallower than those in northern Garden Banks. Continuing to the south, the salt eventually forms vast sheets. Hall (2002) and Jacques and Clegg (2002) suggest that this is a result of an advancing front of salt from the north. The advancing salt front is manifested in Sigsbee Escarpment and Keathley Canyon gorge (Hall, 2002). Since Late Cretaceous, this salt has sealed the deeper sediments and has hindered the upward migration of thermogenic methane through deep-rooted faults (Hall, 2002). However, the active salt migration southward resulted in a heavy deformation in shallow sediments above salt and on the flanks of minibasins where the bulk of gas hydrate reservoir is expected (Frye, 2008).

5.2 Shallow Salt Thermal Impact on GHSZ

The immediate presence of salt can inhibit the stability of gas hydrates in shallow sediments. There are two primary effects. First, the presence of large-scale salt bodies focuses heat into sediments, resulting in higher temperatures so that hydrates cannot form (Yu et al., 1992). Second, the presence of salt in brines may chemically inhibit the occurrence of gas hydrate (Lerche and Noeth, 2002).

The size of the temperature anomaly associated with salt is primarily a function of salt thickness and geometry. These can be precisely determined by mapping the top and bottom of salt layer. While the top salt is relatively easy to map with conventional seismic imaging, the same is not true of the base salt, so there is uncertainty involved in constraining these factors. Here, the thickness of salt was estimated from the overburden thickness (D_{sw}). This is reasonable given that salt diapirs and canopies usually show a thinning toward the edges where salt is partially or completely withdrawn. Withdrawing salt margins are usually deeper than central parts. In the area of this study, salt welds, where salt is totally withdrawn, are encountered more than 2000 deep below seafloor (Hall, 2002) (Figure 14).

Figure 12 shows the relation of the GHSZ thickness to water depth. In areas where shallow salt is absent, the relation follows the curve calculated by Milkov and Sassen (2001). However, since shallow salt is present in most places in the area, the increased heat flow will reduce the thickness of the GHSZ throughout the region. Figure 23 shows a comparison between the shapes of the base of the GHSZ calculated based on the Milkov and Sassen (2001) model (Equation 1) and the salt thermal impact corrected

GHSZ base (Equation 17) on a representative seismic profile. The Milkov and Sassen (2001) line typically is too deep and cuts through areas of shallow salt. Using the model that corrects for the thermal impact of salt (Equation 17), the base of the GHSZ migrates up and away from shallow salt while following the Milkov and Sassen (2001) prediction in areas of deep salt. The difference between the two models is more evident in deep-water areas (Figure 24). Thus, in general, the Milkov and Sassen model tends to over-predict the gas hydrate potential of this region since the predicted base in their scheme is too deep.

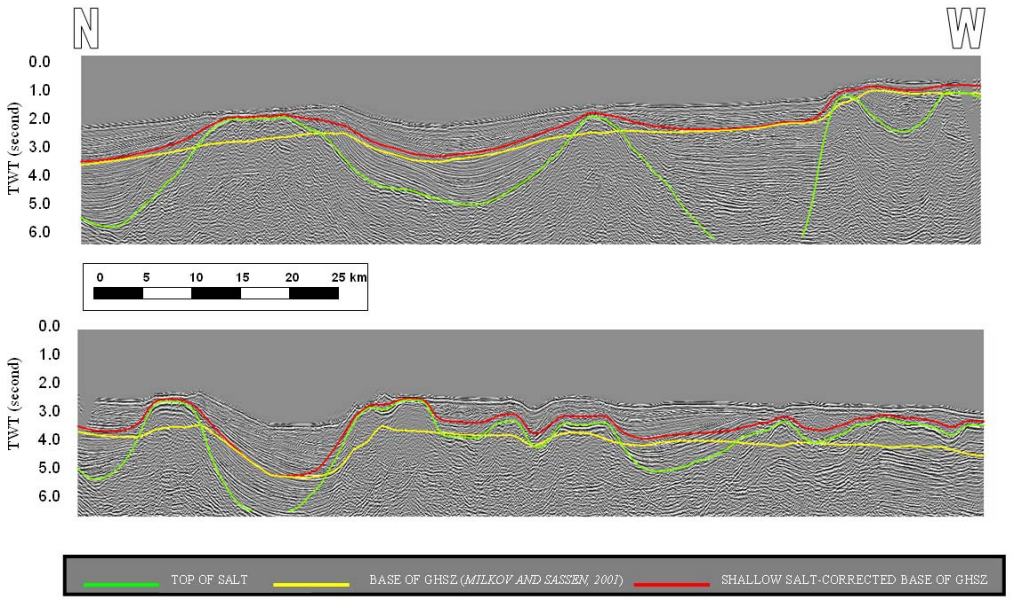

Figure 23. Two cross sections illustrating the difference between the bases of (1) the GHSZ calculated based on the geothermal gradient model of Milkov and Sassen (2001) (yellow line) (Equation 1 and Figure 7) and (2) the GHSZ calculated based on the geothermal gradient model suggested in this study (red line) (Equation 9 and Figure 20). The first base only follows seafloor topography and cross-cuts the top-salt (green line) adding the shallow salt and/or sub-salt sediments below top-salt and above the yellow line to GHSZ. The second base smoothly avoids the top-salt as a result of the thermal impact of shallow salt incorporated in its depth calculation. The deeper the salt below seafloor and/or the deeper the water, the larger the difference in depth between the two bases is. In areas of deep or no salt, the two bases are close in depth.

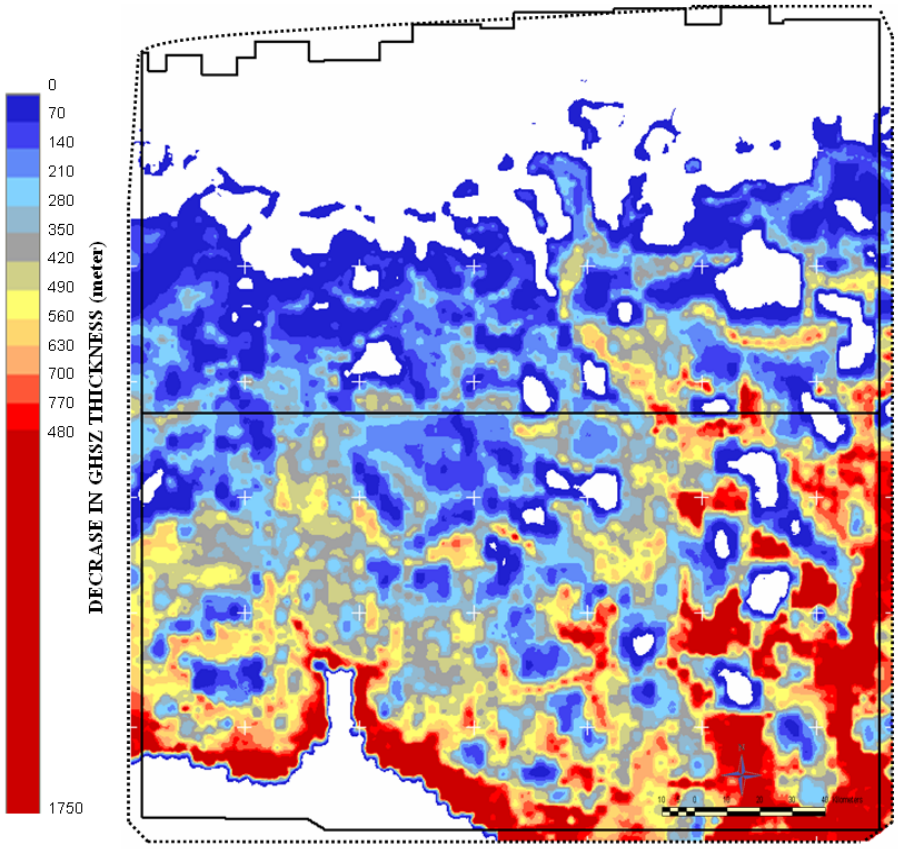

Figure 24. Map of the decrease in thickness of GHSZ as a result of the thermal impact of shallow salt on heat flow. This decrease in thickness was derived from the difference in thickness between the GHSZ thickness calculated based on Milkov and Sassen (2001) (Equation 1) and the GHSZ thickness based on Equation 17.

While the current model clearly improves on the Milkov and Sassen (2001) model in shallow and moderate water depths, in the deepest water areas, we still predict the base of the GHSZ to be below top salt in many areas. In these areas, the predicted temperatures and pressures are such that gas hydrate can be stable even at relatively high temperatures. Figure 21 shows areas where the predicted base of the GHSZ from equation (17) still lies below the top salt. In estimating the potential size of gas hydrate reservoirs, these areas require special consideration.

In calculating the thickness of GHSZ, only the thermal impact of shallow salt was considered. However, salt bodies are a source of brines that have a chemical impact on the occurrence of gas hydrates (Lerche and Noeth, 2002). The primary effect of brine is to inhibit gas hydrate formation. Thus, hydrate will not form in areas immediately adjacent to salt. However, brines can migrate far from salt bodies through continuously fractured zones. Therefore, prediction of gas hydrate concentrations within the GHSZ should be adjusted in sediments where brines are expected.

Brines are expected along active salt-related faults since these faults can act as active conduits. The mapping of contaminated sediments involves understanding the flow system of the whole sediment volume, including the porosity and permeability structure of the region. This is clearly beyond what can be done in a regional study with 2D seismic data and no well control. Nevertheless, mapping the major deformation zones associated with salt tectonics provides a first order understanding of areas where brine solutions that inhibit hydrate formation are likely to found (Figure 18).

Because there is no straightforward way to incorporate these effects into the estimation of the gas hydrate potential, we ignored the effect for now. Instead, we simply subtract out the regions where salt is shallower than the predicted base of the GHSZ. Thus, by combining the results in Figure 21 to the results in Figure 24, we arrive at the final map of the difference between our predicted GHSZ thickness and that predicted by Milkov and Sassen (2001).

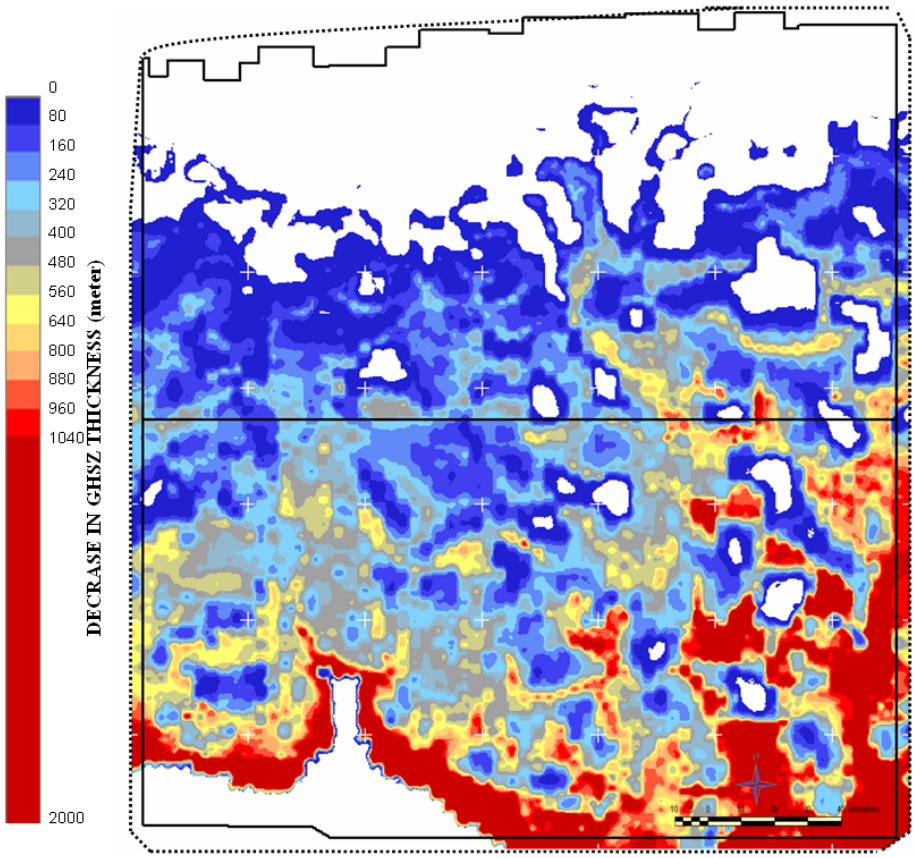

Figure 25: Map of the decrease in thickness of the GHSZ including the thermal and chemical impact of shallow salt. This decrease in thickness was derived from the difference in thickness between GHSZ thickness calculated based on Milkov and Sassen (2001) geothermal gradient model (Equation 1and Figure 7) and GHSZ thickness based on Equation 18 (Figure 22). The difference in thickness between the two GHSZ's includes the difference in thickness in Figure 24 plus the shallow salt and/or sub-salt sediment thickness in Figure 21.

5.3 Distribution and Morphology of Gas Chimneys and BSRs

Salt is thermally conductive and can dramatically affect the overall geothermal system (Ruppel et al, 2005). Heat flow in salt is notably different from the background (Yu et al, 1992; Ruppel et al., 2005). In particular, salt has the effect of focusing heat flow so that near salt, heat flow is significantly greater than background values. Therefore, the immediate presence of salt has a negative effect on adjacent gas hydrate

accumulations. Salt diapirs typically disrupt the GHSZ in the Gulf of Mexico and make it difficult to map BSRs over great distances (Cooper and Hart, 2003; Ruppel et al, 2005). The base of the GHSZ migrates up away from underlying salt layers (Milkov and Sassen, 2001) so that it is no longer parallel to the seafloor, a fact that complicates the detection of BSRs (Geresi et al., 2002; McConnell and Kendall, 2003; Dai et al., 2004).

Figures 26 and 27 show locations of seismic reflections related to possible gas hydrate accumulations detected in this study and their relation to sub-seafloor structures and GHSZ thickness respectively. It also shows locations of interpreted large scale gas chimneys.

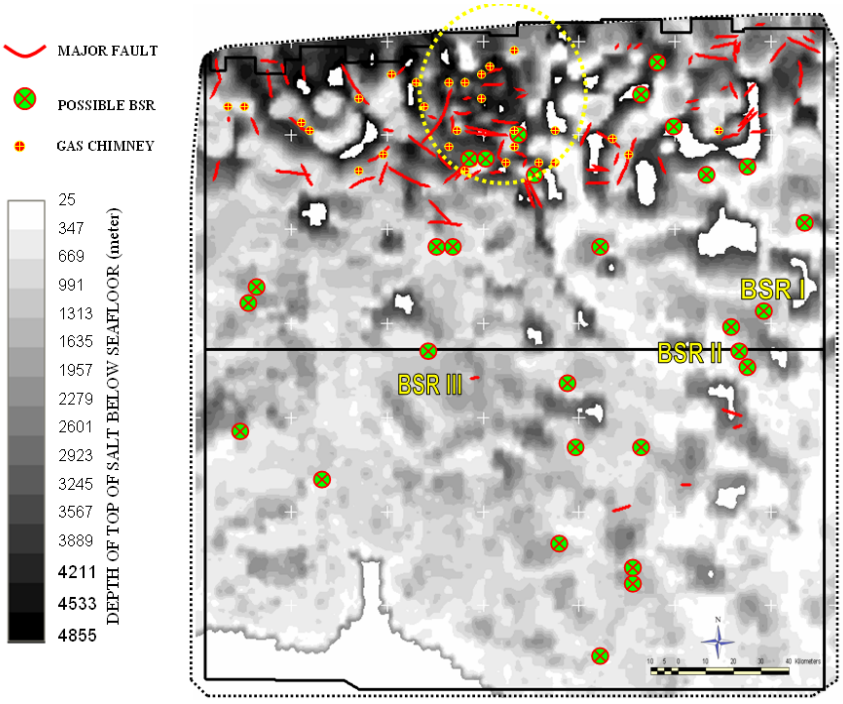

Figure 26. Distribution of gas chimneys and possible BSRs detected in the area imposed on the depth structural map of the top-salt below seafloor. The yellow circle indicates an area of high deformation in shallow sediments by deep-rooted faults and associated shallow-rooted faults. A concentration of gas chimneys and BSRs is observed inside this area. BSRs are mostly detected on shallow salt flanks. BSRs BSR I, BSR II and BSR III are illustrated in cross sections in Figures 29, 30 and 31 respectively.

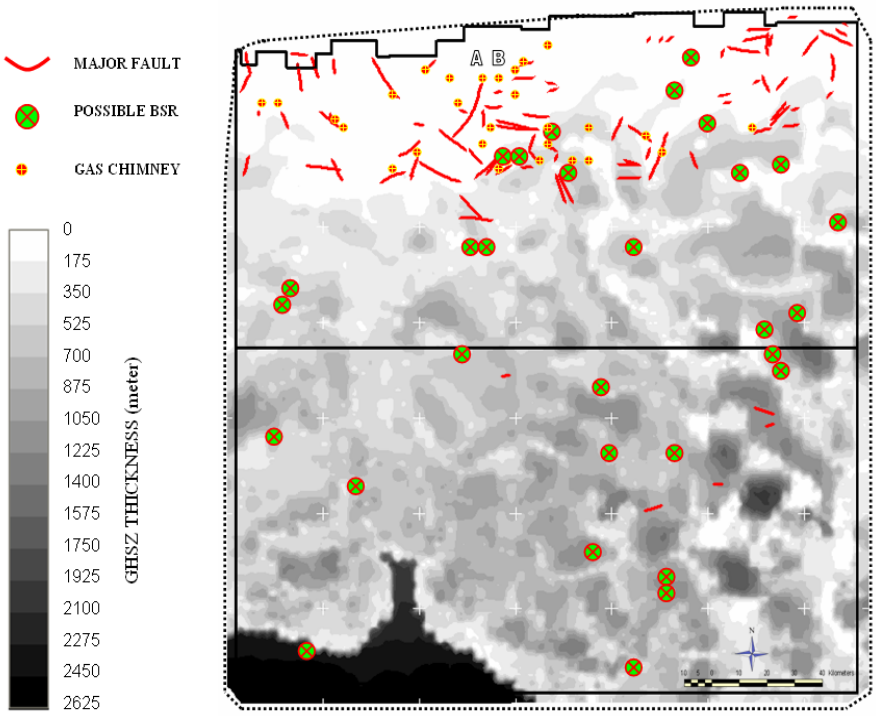

Figure 27. Distribution of gas chimneys and possible BSRs detected in the area imposed on the map of GHSZ thickness. . Gas chimneys A and B are illustrated in a cross section in Figure 28.

Gas chimneys are found almost exclusively in the northern study area where the GHSZ is very thin or non-existent. This is also the region where major fault systems have been mapped. The fault zones likely provide easy migration paths for deep free gas and are further associated with areas of hydrocarbon seepages (Brooks et al, 1986; Milkov and Sassen, 2001). Thus in this region, gas chimneys only form in areas where gas hydrates are unlikely to form except in the very shallowest sediments. In areas where the gas can crystallize into hydrate deep within the sediments, the migration pathways likely become clogged, preventing chimneys from forming. Figure 28 shows two examples of gas chimneys detected in northern Garden Banks. Gas chimneys in this

area can extend for more than 2000 m from seafloor downward. Their diameter may reach up to 4 kilometers. The seafloor hydrate mound at the terminal of the gas chimney may indicate the size of the feeding gas chimney.

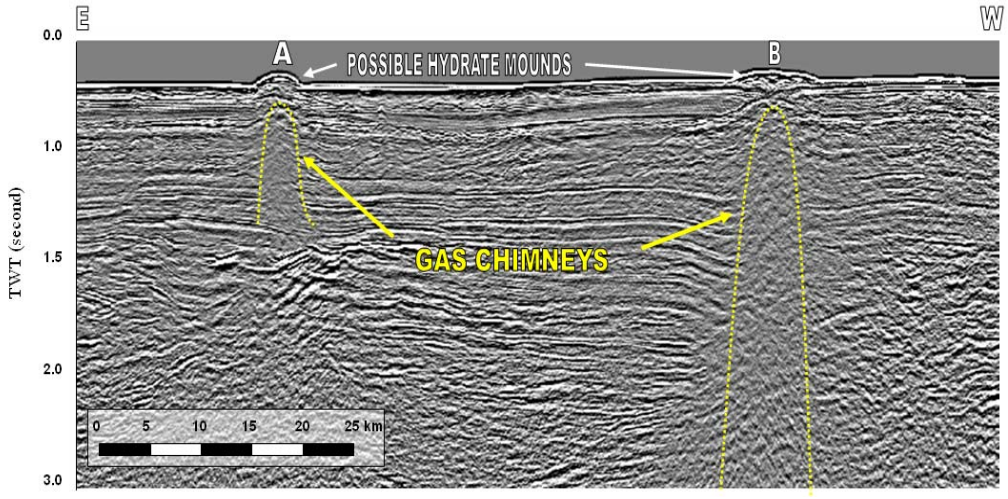

Figure 28. Gas chimneys A and B. These gas chimneys are located in the area of seafloor shallower than the GHSZ upper boundary (see Figure 27 for location). Yellow dotted lines indicate the sediments saturated with free gas. Reflections within gas chimneys are either blurred or migrated down due to the low velocity imposed by the presence of free gas. These gas chimneys feed two possible hydrate mounds on seafloor.

BSRs were mostly detected on deep-water minibasin flanks where shallow sediments are fractured by salt related faults. Figures 29, 30 and 31 show three examples of BSRs detected in the area. They match well (in depth and shape) the calculated base of the GHSZ. These BSRs are traceable for 5-10 kilometers where they merge into stratigraphic reflections and their average depth is around 800 m below seafloor. BSRs detected in northern Gulf of Mexico have similar average depth below seafloor (Hutichnson et al., 2008). The dimmed-out reflections above these BSRs suggest

significant gas hydrate accumulations. Therefore, these BSRs should be the targets of future exploration using seismic and core data. In addition, these examples show that the model developed here provides an excellent first order tool for BSR detection. The match is quite reasonable despite the simplistic nature of the thermal correction in the presence of salt.

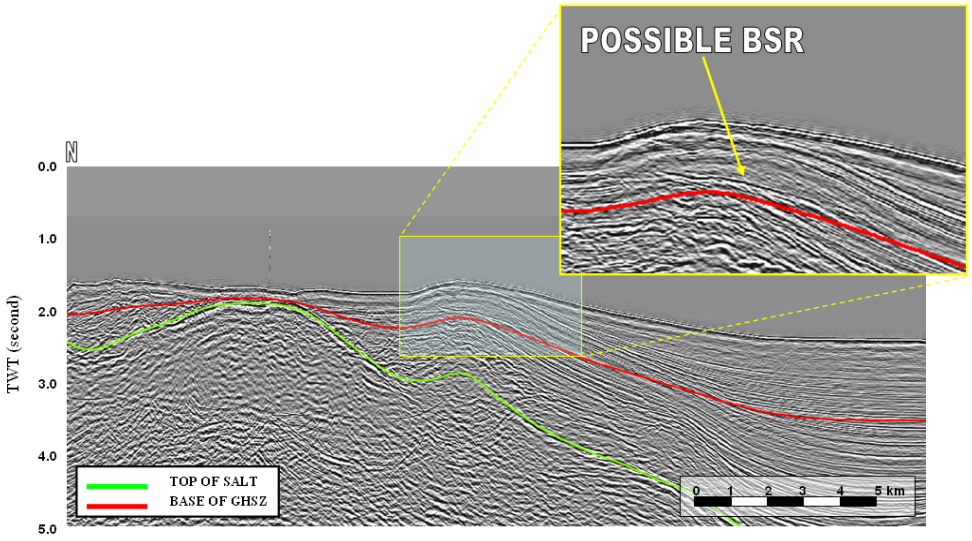

Figure 29. BSR I (see Figure 26 for location) detected on the flank of a minibasin. The reflection is phase-reversed compared to seafloor reflection and matches the modeled base of GHSZ. The BSR crosscuts strata and reflections above the BSR are blurred as an indication of gas hydrates (Dai et al., 2004).

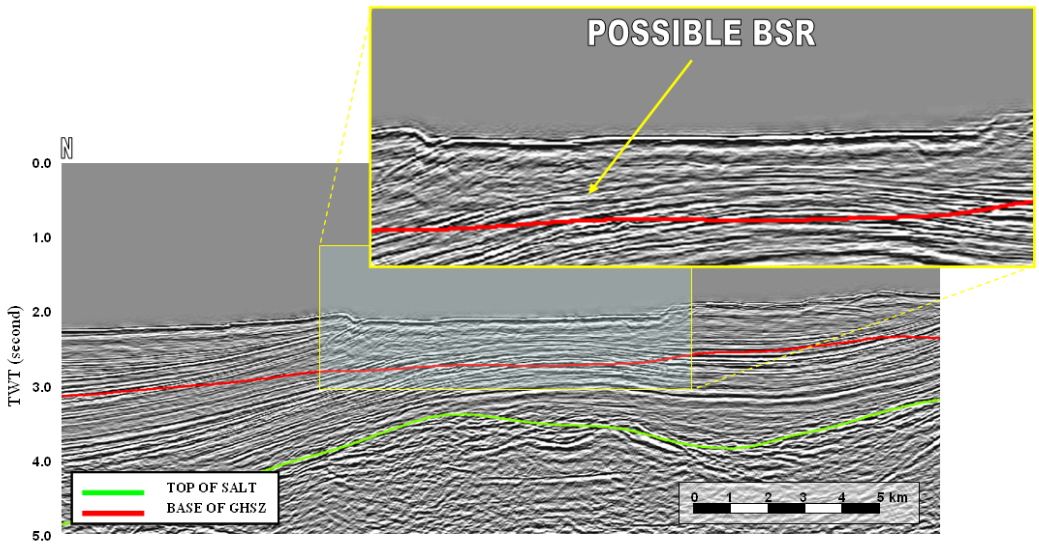

Figure 30. BSR II (see Figure 26 for location) detected on the flank of a minibasin. The reflection is phase-reversed compared to seafloor reflection and matches the modeled base of GHSZ. This BSR crosscuts strata and reflections above the BSR are blurred as an indication of gas hydrates (Dai et al., 2004).

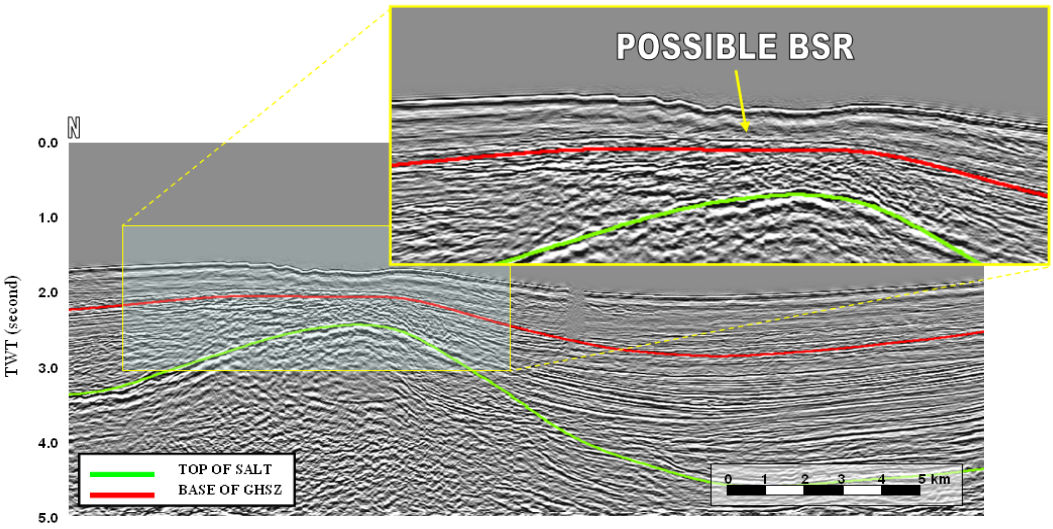

Figure 31. BSR III (see Figure 26 for location) detected on the top of shallow salt sheet. The reflection is phase-reversed compared to seafloor reflection and matches the modeled base of GHSZ. The BSR crosscuts strata and reflections above the BSR are blurred as an indication of gas hydrates (Dai et al., 2004). Following a thermobaric surface (the base of GHSZ) unlike stratigraphic reflections, this BSR is not displaced by shallow faults radiating from the salt sheet.

5.4 Gas Hydrate Concentration and Volume Estimates

From the map of the GHSZ (Figure 22), we can easily calculate the total volume of sediments that are able to host gas hydrate. Given this, we can find the total potential hydrate volume if the concentration is known. This depends on many factors, including methane source, composition and saturation, the porosity and permeability of host sediments, and the salinity of pore-fluids. One of the key factors, however, is the degree to which an area has been affected by faulting (Cooper and Hart, 2003; McConnell and Kendall, 2003; Ruppel et al., 2005). Faults provide pathways for the migration of free gas from deeper hydrocarbon accumulations into the GHSZ (Milkov and Sassen, 2001; Cooper and Hart, 2003; McConnell and Kendall, 2003). Therefore, faults could aid in the accumulation of gas hydrates under the right conditions (Milkov and Sassen, 2001). On the other hand, faults can act as conduits for geothermal heat and brines that dissociate already existing gas hydrate accumulations or prevent the occurrence of such accumulation within the GHSZ (Lerche and Noeth, 2002; Cooper and Hart, 2003; McConnell and Kendall, 2003; Ruppel et al., 2005). Thus faults can have both a positive and negative impact on gas hydrate concentrations in shallow sediments.

From the structural mapping work, the study area can be divided into two distinct domains: minibasins, where little structural deformation is observed and structurally complex areas where shallow salt related faults are common (Figure 18). Previous work in the region suggests that in general, the concentrations are highest in structurally deformed areas and lowest in the minibasin interiors (Prather et al., 2001; Milkov and Sassen, 2001; Cooper and Hart, 2003; Frye, 2008). Following previous authors, we

assume concentrations of 0.1% in minibasin interiors and 0.5% in the highly deformed regions, resulting in a concentration domain map shown in Figure 32.

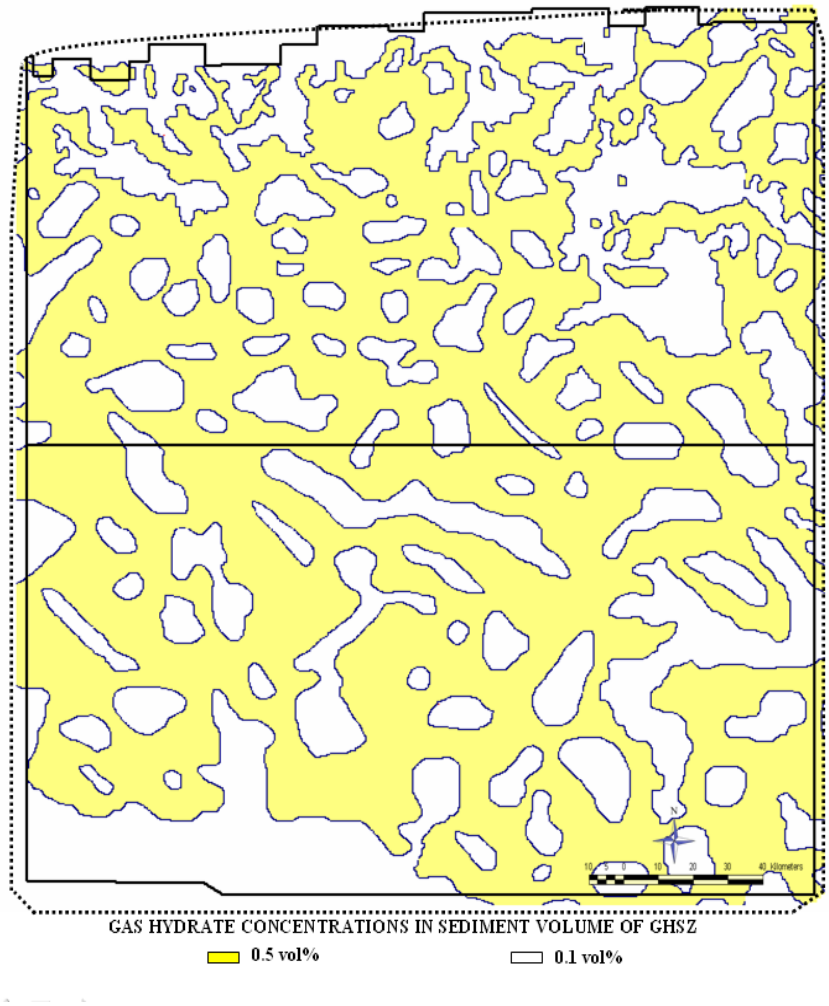

Figure 32. Map of gas hydrate concentrations. Yellow areas are regions of structurally-focused gas hydrates with a concentration of around 0.5 vol.%. White areas are minibasin interiors with a gas hydrate concentration of around 0.1 vol.%. Distribution of these two gas hydrate concentrations was based on shallow sediments deformation zones in Figure 18.

The total volume of sediments in the GHSZ is 24.5×10^{12} m^3, of which 21.5×10^{12} m^3 is found in the minibasin interiors. Combined with the above concentration estimates,

the total volume of gas hydrate in this region is 39×10^9 m^3, of which 21.5×10^9 m^3 is in the minibasin interiors. Thus, even though the concentrations are generally higher in the structurally deformed regions, the smaller areal extent and thinner GHSZ in these regions means that less than half of the total hydrate volume will be found there.

Assuming that methane is the only gas found in gas hydrates in this area, one cubic meter of gas hydrate provides around 140 cubic meters of methane at standard temperature and pressure conditions (Collet, 1995). Converting the total volume of gas hydrate into methane, the Garden Banks and Keathley Canyon region can theoretically provide around 5.5×10^{12} m^3 of pure methane. This works out to 120 cubic meters of methane per square meter for the region.

The map of gas hydrate potential distribution summarizes the quantitative results of this study (Figure 33). The map is a combination of the GHSZ thickness map in Figure 22 and the gas hydrate concentration map in Figure 32. This map shows the volume of gas hydrate theoretically found below each square meter of seafloor. The gas hydrate volume below each square meter cell is a direct function of GHSZ thickness and gas hydrate concentration. Thus, the map shows the distribution of the potential gas hydrate reservoir throughout the area and reflects the probability of finding gas hydrate accumulations in shallow sediments. It combines the impact of major structural, thermal, and chemical factors on the occurrence of gas hydrates.

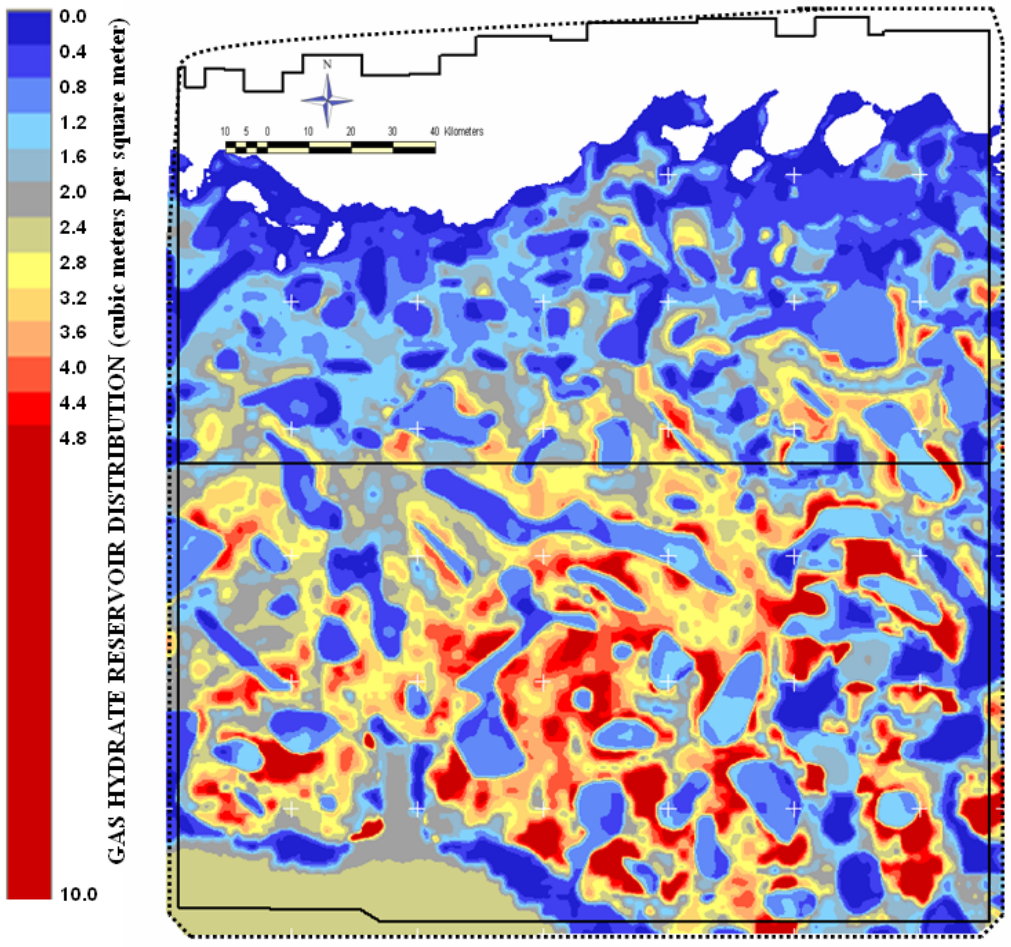

Figure 33. Map of the gas hydrate reservoir volume distribution (gas hydrate volume in cubic meters theoretically found in sediments below each square meter cell of seafloor).

Gas hydrate is estimated to occur from zero to ten cubic meters per square meter. In the northern Garden Banks, there is very small to no gas hydrate potential. This is due to the thin or absent GHSZ in the area as well as very little deformation in the shallow sediments. In the southern Garden Banks, a thin GHSZ is balanced by the high concentrations of gas hydrate associated with strong shallow sediment deformation, making this area a possible source of valuable gas hydrate accumulations.

In the Keathley Canyon area north of Sigsbee Escarpment, there are two distinct domains of gas hydrate occurrence:(1) areas of high probability, two to five and up to ten cubic meters per square meter, where the GHSZ is thick and shallow sediments are heavily deformed; and, (2) areas of low gas hydrate probability, less than one cubic meter per square meter, associated with deep water minibasins but with little deformation in shallow sediments. In Keathley Canyon, the probability is more affected by the degree of deformation in shallow sediments. The first domain holds the bulk of gas hydrate potential in the study area.

In the area approaching the Sigsbee Escarpment, the salt layer becomes very shallow. Subsequently, a thin GHSZ is predicted. This area is characterized by little probability of gas hydrate occurrence. This area is a good example of the impact of thick shallow salt on deepwater gas hydrate occurrences.

In areas south of Sigsbee Escarpment (2000-3000 m water depth where no shallow salt is detected), we estimate two and half cubic meters of gas hydrate per square meter. The area has a thick GHSZ (1200-2500 m thick) but low thermogenic gas hydrate concentrations are expected.

5.5 Methane Hydrate Potential in Northern Gulf of Mexico

To get an idea of the total methane hydrate potential of the northern Gulf of Mexico, the estimation of 120 cubic meters of methane per square meter of seafloor from Garden Banks/Keathely Canyon was extrapolated to the entire outer continental shelf (Figure 34). Although this is obviously a crude estimate, the outer shelf has similar water depths

(around 100-3100 m deep) and a similar layer of thick shallow salt. The outer shelf area is around 450,000 square kilometers, resulting in $55x10^{12}$ m^3 of methane that is theoretically extractable from the shallow sediments. By comparison, the proven natural gas reserves in federally regulated parts of the Gulf of Mexico are only around $5x10^{12}$ m^3, of which 80% has already been produced as of 2002 (Crawford et al., 2005). Thus, the volume of methane stored in the gas hydrates offshore Gulf of Mexico is a huge potential fuel reservoir.

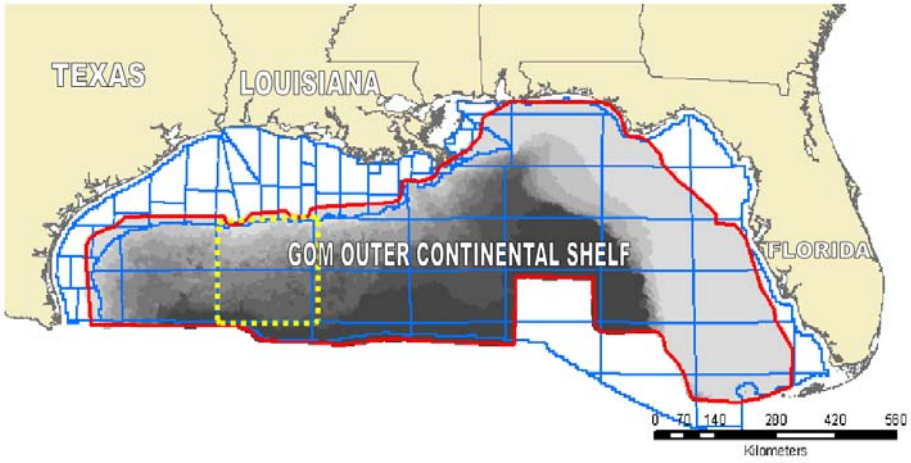

Figure 34. The outer continental shelf of the northern Gulf of Mexico (after Frye, 2008). Red line is the MMS defined boundary (450,000 square kilometers). Blue regions are the MMS protraction areas. The yellow square covers the Garden Banks and Keathley Canyon blocks, from which gas hydrate reservoir statistics were extrapolated to the whole shelf.

6. CONCLUSIONS

In this work, we investigated the gas hydrate potential of the Garden Banks and Keathley Canyon areas offshore Gulf of Mexico. The region contains significant salt deposits that have a large impact on the stability of gas hydrate. Shallow salt divides the sub-seafloor structure into many minibasins surrounded by walls of salt. Salt affects the gas hydrate stability zone by altering the local temperature and chemical structure of shallow sediments. In addition, deformation of shallow sediments in response to salt tectonics has a large impact on fluid and gas migration pathways.

To estimate the gas hydrate potential, we first mapped the salt throughout the region. From this, we derived a simple correction to the temperature field in the shallow sediments to estimate the depth to the base of hydrate stability zone. Deep water shallow sediments in Garden Banks and Keathley Canyon areas have a high potential for stable gas hydrate presence. Comparing the predicted base to the 2D seismic data available, we found several examples of gas hydrate indicators, including bottom simulating reflectors and gas chimneys. These direct hydrate indicators give us confidence that the method can be used to place first order constraints on the total volume of sediment that can potentially host gas hydrate.

Combined with previous work in the region where the concentration of gas hydrate hosted in sediments has been estimated, we were then able to calculate the size of the gas hydrate reservoir and estimate the total amount of methane. High gas hydrate concentrations are most likely to occur on deepwater minibasin flanks were thick GHSZ

and fractured shallow sediments are common. A total of 5.5 trillion cubic meters of hydrate methane is predicted in this area.

REFERENCES

Brooks, J., M. C., Kennicutt II, R. R. Fay, T. J. McDonald, and R. Sassen, 1984, Thermogenic gas hydrates in the Gulf of Mexico: Science, **225**, 409-411.

Brooks, J. M., H. B. Cox, W. R. Bryant, M. C. Kennicutt II, R. G. Mann, and T. J. MacDonald, 1986, Association of gas hydrates and oil seepage in the Gulf of Mexico: Organic Geochemistry, **10**, no.1-3,221-234.

Bryant, W. R., J. R. Bryant, M. H. Feeley, and G. R. Simmons, 1990, Physiographic and bathymetric characteristics of the continental slope of northwest Gulf of Mexico: Geo-marine Letters, **10**, no. 4, 182-199.

Bünz, S., J. Mienert, M. Vanneste, K. Andreassen, 2005, Gas hydrates at the Storegga Slide: Constraints from an analysis of multicomponent wide-angle seismic data: Geophysics, **70**, no. 5, B19-B34.

Collett, T. S., 1995, Gas hydrate resources of the United States, *in* D. L. Gautier, G. L. Dolton, K. I. Takahashi, and K. L. Varnes, eds., National Assessment of United States Oil and Gas Resources — Results, Methodology, and Supporting Data: US Geological Survey Digital Data Series 30, p. 78.

Cooper, A. K., and P. E. Hart, 2003, High-resolution seismic-reflection investigation of the northern Gulf of Mexico gas hydrate stability zone: Marine and Petroleum Geology, **19**, 1275-1293.

Crawford, T. G., G. L., Burgess, C. J. Kinler, M. T. Prendergast, K. M. Ross, K.M., N. K. Shepard, 2005, Estimated oil and gas reserves, Gulf of Mexico, December 31, 2002: OCS Report MMS 2005-052.

Dai, J., H. Xu, F. C. Snyder, N. Dutta, 2004, Detection and estimation of gas hydrates using rock physics and seismic inversion: Examples from the northern deepwater Gulf of Mexico: The Leading Edge, **23**, 60-66.

Deuflhard, P., 2004, Newton methods for nonlinear problems. Affine invariance and adaptive algorithms: Springer Series in Computational Mathematics, vol. 35.

Forrest, J., E. Marcucci, P. Scott, 2005, Geothermal gradients and subsurface temperature in the northern Gulf of Mexico: Transactions of the Gulf Coast Association of Geological Societies, **55**, 233-248.

Frye, M., ed., 2008, Preliminary evaluation of in-place gas hydrate resources: Gulf of Mexico Outer Continental Shelf: OCS Report MMS 2008-004, accessed October 6, 2008;

http://www.mms.gov/revaldiv/GasHydrateFiles/MMS2008-004.pdf.

Geresi, E., C. Lutken, T. McGee, T., and A. Lowrie, 2002, Complex geology and gas hydrate dynamics characterize Mississippi Canyon Block 798 on the upper continental slope of the northern Gulf of Mexico, *in* S. P. Dutton, S. C. Ruppel, and T. F. Hentz, eds., Transactions of the Gulf Association of Geological Societies, **52**, 309-321.

Hall, S. H., 2002, The role of autochthonous salt inflation and deflation in the northern Gulf of Mexico: Marine and Petroleum Geology, **19**, 649–682.

Heggland, R., W. W. Sager, W. R. Bryant, and E. H. Doyle, 2004, Definition of geohazards in exploration 3D seismic data using attributes and neural-network analysis: The American Association of Petroleum Geologists Bulletin, **88**, no. 6, 857-868.

Hutchinson, D. R, C. Ruppel, H. S. Roberts, R. S. Carney, M. A. Smith, 2008, Gas hydrates in the Gulf of Mexico, *in* C. W. Holmes ed., Gulf of Mexico – Its Origin (History, Archeology and Geology), vol. 1: Texas A&M University Press.

Jacques, J. M., and H. Clegg, 2002, Late Jurassic source rock distribution and quality in the Gulf of Mexico: Inferences from plate tectonic modeling: Transactions of the Gulf Coast Association of Geological Societies, **52**, 429-440.

Jensen, L. N., and K. Sørensen, 1992, Tectonic framework and halokinesis of the Nordkapp Basin, Barents Sea, *in* R. M. Larsen H. Brekke, B. T. Larsen, and E. Talleraas, eds., Structural and Tectonic Modeling and Its Application to Petroleum Geology: Norwegian Petroleum Society (NPF) Special Publication 1, Elsevier, 109-120.

Jones, M., S. Nagihara, S., M. Smith, 2003, The regional geothermal heat flow regime of the North-Central Gulf of Mexico Continental Slope: Transactions of the GCAGS, **53**, 363-373.

Kvenvolden, K. A., 1993, Gas hydrates as a potential energy resource-A review of their methane content, *in* D. G. Howell, ed., The Future of Energy Gases: US Geological Survey Professional Papers 1570, 555-561.

Kvenvolden, K.A., and M. A. McMenamin, 1980, Hydrates of natural gas: A review of their geologic occurrence: US Geological Survey Circular 825, p. 14.

Lawver, L. A., A. Grantz, and L. M. Gahagan, 2002, Plate kinematic evolution of the present Arctic region since the Ordovician, *in* E. L. Miller, A. Grantz and S. L. Klemperer eds., Tectonic Evolution of the Bering Shelf - Chukchi Sea - Arctic Margin and Adjacent Landmasses: Geological Society of America Special Paper, 333-358.

Lerche, I., and S. Noeth, 2002, Hydrate composition determination from seismic data: An inverse procedure: Energy Exploration & Exploitation, **20**, 51-88.

Lowrie, A., R. Hamiter, M. D. Max, I. Lerche, and E. Bagirov, 1997, Hydrate stability zone permanence along dynamic Louisiana offshore: Transactions of the Gulf Coast Association of Geological Societies, **47**, 311-315.

McConnell, D. R., and B. A. Kendall, 2003, Images of the base of gas hydrate stability in the deepwater Gulf of Mexico; Examples of gas hydrate traps in the northwest Walker Ridge and implications of successful well planning: The Leading Edge, **22**, no. 4, 361-367.

Milkov, A. V., and R. Sassen, R., 2001, Estimate of gas hydrate resource, northwestern Gulf of Mexico continental slope: Marine Geology, **179**, 71-83.

Minerals Management Service, 2005, Geographic mapping data in digital format, http://www.gomr.mms.gov/homepg/pubinfo/repcat/arcinfo/index.html, accessed October 6, 2008.

Prather, B. E., J. R. Booth G. S. Steffens, and P. A. Craig, 1998, Classification, lithologic calibration and stratigraphic succession of seismic facies from intraslope basins, deep water Gulf of Mexico, USA: The American Association of Petroleum Geologists Bulletin, **82**, no. 5, 701–728.

Ray, P. K., 1988, Hydrocarbon potentials of the deepwater (600 feet) Gulf of Mexico: Proceedings of the MTS/IEEE Conference, 622-627.

Ruppel C., G. R. Dickens, D. G. Castellini, W. Gilhooly, and D. Lizarralde, 2005, Heat and salt inhibition of gas hydrate formation in the northern Gulf of Mexico: Geophysical Research Letters, **32**, 4.

Salvador, A., 1987, Late Triassic-Jurassic paleogeography and origin of Gulf of Mexico basin: The American Association of Petroleum geologists Bulletin, **71**, no. 4, 419-451.

Schlumberger, 2003, Theoretical modeling and analysis for gas hydrate quantification from prestack seismic data in the northern deepwater Gulf of Mexico: Chevron Texaco Gas Hydrate JIP Report, accessed October 6, 2008; http://204.154.137.14/technologies/oil-gas/publications/Hydrates/pdf/Project_pdfs/GasHydratesJIPFinalReportV1.pdf.

Shipley, T. M. Houston, R. Buffler, F. Shaub, K. McMillen, J. Ladd, and J. Worzel, 1979, Widespread occurrence of possible gas hydrate horizons from continental slope as identified on seismic reflection profiles: Proceedings of the 11th Offshore Tech. Conference, **11**, no. 3, 1879-1886.

Sloan, E. D., Jr., (1998) Clathrate hydrates of natural gases. Second edition: Marcel Dekker Inc.

Snyder, F. C., L. K. Muller, N. Dutta, D. R. Hutchinson, P. E. Hart, M. W. Lee, B. Dugan, C. Ruppel, W. T. Wood, R. Coffin, R. Evans, and E. H. Jones, 2004, Seismic analysis and characterization of gas hydrates in the northern deepwater Gulf of Mexico: The Annual Meeting of the American Association of Petroleum Geologists, **88**, no. 13.

TGS-NOPEC, 2004, 2D Data Library, http://www.tgsnopec.com/data_library/dataLibrary.asp?mid=155, accessed January 15, 2007.

Trudgill, B. D., M. G. Rowan, J. C. Fiduk, P. Weimer, P. E. Gale, B. E. Korn, R. L. Phair, W. T. Gafford, G. R. Roberts, and S. W. Dobbs, 1999, The Perdido Fault Belt, northwestern deep Gulf of Mexico, Part 1: Structural geometry, evolution and regional implications: The American Association of Petroleum Geologists Bulletin, **83**, 88-113.

Watkins, J., and R. T. Buffler, 1996, Gulf of Mexico: Deepwater frontier exploration potential, *in* J. O. Jones and R. L. Freed, eds., Structural Framework of the

Northern Gulf of Mexico: Gulf Coast Association Geological Societies Special Publication, 79-92.

Winters, B., and T. Lorenson, 2002, Gas hydrate studied in the Northern Gulf of Mexico: US Geological Survey, accessed January 15, 2007; http://soundwaves.usgs.gov/2002/09/.

Yu, Z., I. Lerche, and A. Lowrie, 1992, Thermal impact of salt: Simulation of thermal anomalies in the Gulf of Mexico: Pure and Applied Geophysics, **138**, 181–192.

VITA

Name:	Idris Murad
Address:	The Department of Geology and Geophysics, Texas A&M University, College Station, Texas 77843-3115.
Email Address:	iiidriiis@yahoo.com
Education:	B.S., Geophysics, Damascus University, 2002 M.S., Geophysics, Texas A&M University, 2009